Chitosan-alginate polyelectrolyte complexes for encapsulation of low molecular weight fish bioactive peptides

Yoni Atma [a,b], Amin Sadeghpour [a], Brent S. Murray [a,*], Francisco M. Goycoolea [a,c]

[a] *School of Food Science and Nutrition, University of Leeds, LS9 2JT, UK*
[b] *Department of Food Science and Technology, Faculty of Bioindustry, Universitas Trilogi, Jakarta, 12760, Indonesia*
[c] *Department of Cell Biology and Histology, Faculty of Biology, University of Murcia, 30100, Murcia, Spain*

ARTICLE INFO

ABSTRACT

Encapsulation of low molecular weight (M_w) bioactive peptides (BAPs) in electrostatically mediated polyelectrolyte complexes (PECs) of sodium alginate (ALG) and chitosan (CS) was studied, formed via a simple one-step mixing process. PECs were characterized via dynamic light scattering (DLS), mixed-mode phase analysis light scattering (M3-PALS), static light scattering (SLS), small-angle X-ray scattering (SAXS) and transmission electron microscopy (TEM). The encapsulation efficiency (EE) and *in vitro* release of low M_w antihypertensive LKPNM and LKP BAPs (derived from fish hydrolysates) were measured, under both gastric and intestinal pH conditions, via high performance liquid chromatography (HPLC). Two different ALG were tested ($M_w \approx 8$ and 21 kDa, with mannuronic: guluronic ratios 5.1 and 1.4, respectively), whilst the M_w and degree of acetylation (DA) of the CS were ≈ 111 kDa and ≈ 10 %, respectively. At the pH (5.5) of PEC formation the BAPs were positively charged. As the molar charge ratio of alginate to chitosan (n^-/n^+) was increased from 0.1 to 0.6 the PEC size reduced from *ca.* 800 to 300 ± 50 nm, indicating more compact structures, but increased again significantly to >10 μm around charge neutralisation ($n^-/n^+ = 1$) and net PEC ζ-potential swapping from +ve to –ve. The size then decreased again to between 1 and 10 μm as $n^-/n^+ \to 10$, as expected if the more prevalent polysaccharide (ALG) coated the surface of the PECs. However, higher M_w ALG gave significantly smaller (more compact) and more highly negatively charged PECs for $n^-/n^+ > 1$. The PECs showed high ($\approx 80\%$) EE but low (10–20%) release in gastrointestinal conditions, highlighting their potential as effective carriers of such BAPs.

1. Introduction

Bioactive peptides (BAPs), typically composed of 2–20 amino acids, exhibit bioactivities relating to disease prevention, promotion of human health and support of physiological functions (Atma et al., 2024; Guo et al., 2023; Nongonierma & FitzGerald, 2015; Patil et al., 2022). The majority of BAPs are derived from enzymatically hydrolyzed proteins (Han et al., 2021; Lorenzo et al., 2018) sourced from natural materials such as dairy products (Estévez et al., 2020; Nongonierma et al., 2019; Yan et al., 2019), meat (Cao et al., 2020; Xing et al., 2019), fish (Abdelhedi et al., 2017; Neves et al., 2017), eggs (Marcet et al., 2022; Moreno-Fernández et al., 2020), plant proteins (Han et al., 2019; Kumar et al., 2022; Piovesana et al., 2018; Yuan et al., 2022), algae (Cermeño et al., 2020; Harnedy et al., 2017), insects (Ma et al., 2023; Sousa et al., 2020), and mushrooms (Zhou et al., 2020). Fish and by-products from fish processing stand out as potent sources of BAPs, exhibiting

bioactivities encompassing antioxidant, antihypertensive, antimicrobial, and anti-inflammatory properties (Gao et al., 2021; Halim et al., 2016; Le Gouic et al., 2019; Nirmal et al., 2022; Zamora-Sillero et al., 2018). Notably, marine sources seem to surpass antihypertensive BAPs from other sources, with some supplements containing these BAPs being commercially available (Fuentea et al., 2020; Hayes & Tiwari, 2015). The burgeoning interest in fish BAPs underscores their potential to enhance health and prevent diseases and a significant advance in the development of functional foods and nutraceuticals.

A notable antihypertensive BAP with pronounced bioactivity is the pentapeptide LKPNM (leucine-lysine-proline-asparagine-methionine), derived for example from the muscle of bonito fish (*Sarda* spp.) via thermolysin hydrolysis. This BAP, presented in the form of a food supplement (Curtis et al., 2002; Fujita & Yoshikawa, 1999), has been patented, one advantage of it being that LKPNM does not exhibit a bitter taste (Yokoyama et al., 1992). However, it is noteworthy that, to date,

---

there is a dearth of published research on the encapsulation of this particular BAP. It is widely acknowledged that encapsulation of BAPs for applications in food, food supplements, and nutraceuticals is imperative to shield them from undesired hydrolysis and degradation during normal digestion, to preserve their sequences and bioactivities (Basirico et al., 2015; Fernández-Musoles et al., 2013; Lacroix et al., 2017). Prior investigations have predominantly centered on the encapsulation of insulin, proteins or protein fragments considerably larger than the above defined M_w range (Aguilar-Toala et al., 2022; Feng et al., 2019; Goycoolea et al., 2009; Mohan et al., 2016; Mohan et al., 2015; Zhang et al., 2021) often by at least tenfold. Some attempts have been made to encapsulate BAPs ranging from di-to decapeptides, notably using chitosan (CS) as an encapsulating material (Bicak et al., 2021; Chen et al., 2017; Danish et al., 2017), or chitosan combined with alginate (ALG). The composite material serves as an effective carrier under a range of conditions, mitigating premature release of BAPs (Huang et al., 2017; Laroui et al., 2010; Xiao et al., 2017).

Chitosan (CS) is a cationic polysaccharide obtained from chitin, which in turn is one of the most abundant biopolymers in nature, found in the exoskeleton of crustaceans such as crab and shrimp and also in molluscs, insects and fungi. CS is produced on a commercial scale by partial thermoalkaline N-deacetylation of chitin (Alonso & Goycoolea, 2008) and is relatively inexpensive (George & Abraham, 2006). CS structure is a linear polysaccharide consisting of glucosamine (deacetylated units, D) and N-acetyl-glucosamine (acetylated units, A) units linked via β-(1 → 4) linkages (Potaś et al., 2020) (see Fig. 1a). The ratio of the mole fraction of A residues to the total (A + D), defines the degree (or fraction) of acetylation (DA). The distribution of A residues in CS, known as the pattern of acetylation, in chemically deacetylated CS is known to be random but using enzymatic technology it is possible to produce block-wise patterned CS (Wattjes et al., 2020). The other parameter that dictates CS properties and applications is the M_w distribution (in particular, the ratio of the weight average M_w to the number average M_w, also referred to as the polydispersity index). The intrinsic pK_a (pK_0) of the CS, known to be independent of CS's degree of neutralisation and degree of acetylation (up to DA ~25%), has been determined as 6.0 ± 0.1 (Rinaudo et al., 1999a, 1999b). At pH values of ≈6.0 and below, corresponding to a minimum degree of protonation of 0.5, CS dissolves in dilute acidic aqueous solutions. Generally, commercial CS shows DA values between ~0.05 and ~0.30 and M_w values between ~10 and ~500 kDa (Luo & Wang, 2014).

CS has been widely used in the food and pharmaceutical industries. CS has superior properties as an encapsulation agent, particularly for oral or gastrointestinal delivery, because it is biodegradable, biocompatible, mucoadhesive, a permeation enhancer and easy to modify. CS increases the bioaccessibility and bioavailability of encapsulated proteins and peptides during gastrointestinal delivery because its mucoadhesive ability facilitates penetration into the intestinal mucus layer. CS encourages opening of the tight junctions and therefore absorption via the paracellular route in the intestinal epithelium (Sonaje et al., 2012). Due to its positive charge at mildly acidic conditions CS forms complexes with polyanions such as alginate (ALG) by means of electrostatic interactions that can aid delivery (Potaś et al., 2020). Polyelectrolyte complexes (PECs) have been the subject of extensive research, serving as one of prominent methods for encapsulating and delivering bioactive proteins and peptides (Kulkarni et al., 2016).

ALG is an anionic polysaccharide that is commercially extracted from brown seaweeds. ALG is an unbranched biopolymer consisting of (1 → 4) linked α-guluronic acid (G) and β-mannuronic acid (M) in blocks of various lengths (Goycoolea et al., 2009). There can be homosequences (M blocks or G blocks) interspersed with heterosequences (G-M blocks) of various lengths (see Fig. 1a) with overall M_w typically between 60 and 700 kDa. The charged carboxyl groups make ALG highly water soluble but also capable of forming gels by decreasing the pH (protonating the COO⁻ groups) or by addition of specific divalent cations such as Ca^{2+} to form Ca-ALG (Stewart & Swaisgood, 1993; Tanaka et al., 1984). The

mannuronic to guluronic (M/G) ratio and M_w also affect the physical properties of ALG (Cazorla-Luna et al., 2021). ALG has been used extensively by the food industry and has GRAS (Generally Recognized as Safe) approval by the FDA. Recently ALG has been developed as microgel particles and the protein lactoferrin encapsulated via a simple one step precipitation process (Pravinata et al., 2016).

In terms of an encapsulation agent for gastrointestinal delivery, ALG offers many advantages. Like CS, these include its mucoadhesive character (George & Abraham, 2006; Gombotz & Wee, 1998), low toxicity, biocompatibility and the fact that it is not hydrolyzed by most enzymes in the gastrointestinal tract. As mentioned above, its anionic charge makes it ideal for formation of a polyelectrolyte complex (PEC) with the cationic polymer CS. Such PECs can trap BAPs within them and aid their protection and delivery. For example, some studies have proven that crosslinking ALG with CS reduces the porosity of ALG hydrogels that prevents BAP leaching under gastric conditions (George & Abraham, 2006; Luo & Wang, 2014; Potaś et al., 2020). CS + ALG systems have been used to encapsulate the BAP KPV via a double emulsion solvent evaporation method (Xiao et al., 2017) and to encapsulate the peptide VLPVP via membrane emulsification and ionic gelation (Huang et al., 2017). The apparent simplicity and versatility of PECs based on CS + ALG combinations would seem to make them an ideal candidate for delivery of BAPs and this study explores a model system in detail to try to understand the key factors controlling their formation, encapsulation efficiency and BAP release.

2. Materials and methods

2.1. Materials

Chitosan (CS) (product code HMC 90/100, batch number 212-160315-03) with a M_w of 111 kDa (polydispersity = 1.2) as determined by HPSEC-MALS-RI-UV/VIS (see Supplementary Material), intrinsic viscosity ([η]) ~ 400 mL g⁻¹ (as determined by viscometry in 20% acetic acid and 85 mM NaCl, 25 °C) and degree of acetylation (DA) = 10 %, as determined by ¹H NMR spectroscopy (Hirai et al., 1991), was obtained from Heppe Medical Chitosan GmbH (Halle, Germany).

Sodium alginate of M_w 21 kDa (ALG21), with a mannuronic (M) to guluronic (G) acid (M/G) ratio = 1.42 and sodium alginate of M_w 8 kDa (ALG8), M/G ratio = 5.1 were obtained from and characterised by Danisco, (Copenhagen, Denmark). The samples belong to the same panel of samples used in previous studies (Fuenzalida et al., 2016; Goycoolea et al., 2009). Bonito fish protein extract (PeptACE®) was obtained from Natural Factors (Washington, USA). Synthetic peptide standards LKPNM and LKP (≥95% HPLC) were obtained from GenScript (Oxford, UK). Acetonitrile (ACN) (HPLC grade), salt (NaCl), hydrochloric acid and sodium azide were purchased from Sigma-Aldrich (Gillingham, UK); trifluoroacetic acid (TFA) (HPLC grade 99.5%) from Alfa Aesar (Heysham, UK). Ultrapure Milli-Q water was provided by a Milli-Q apparatus (Millipore Corp., Bedford, MA, USA) and used to make up all solutions unless otherwise stated. A Hettich, Ritona 380 R centrifuge (A Hettich, Tuttlingen, Germany) was used to centrifuge (2 mL) the various samples throughout.

2.2. BAP isolation from protein extract

PeptACE® powder (2 g) was dissolved in 100 mL of water and stirred with an IKA RT 5 magnetic stirrer (Oxford, UK) at 250 rpm at 25 °C for 60 min. The solution was then centrifuged at 5000×g for 30 min at 4 °C. The supernatant was then filtered through an Ultracel® ultrafiltration disc with 3 kDa M_w cut off (Amicon® Bioseparations, Massachusetts, USA). The filtered solution was then stored (for 1 week) at 4 °C before further purification and analysis via high-performance liquid chromatography (HPLC). A Shimadzu HPLC with a UFLC-XR system (Kyoto, Japan) was used in reverse-phase (RP) mode. The filtered solution was diluted 10 x with water then passed through a 0.22 μm hydrophilic
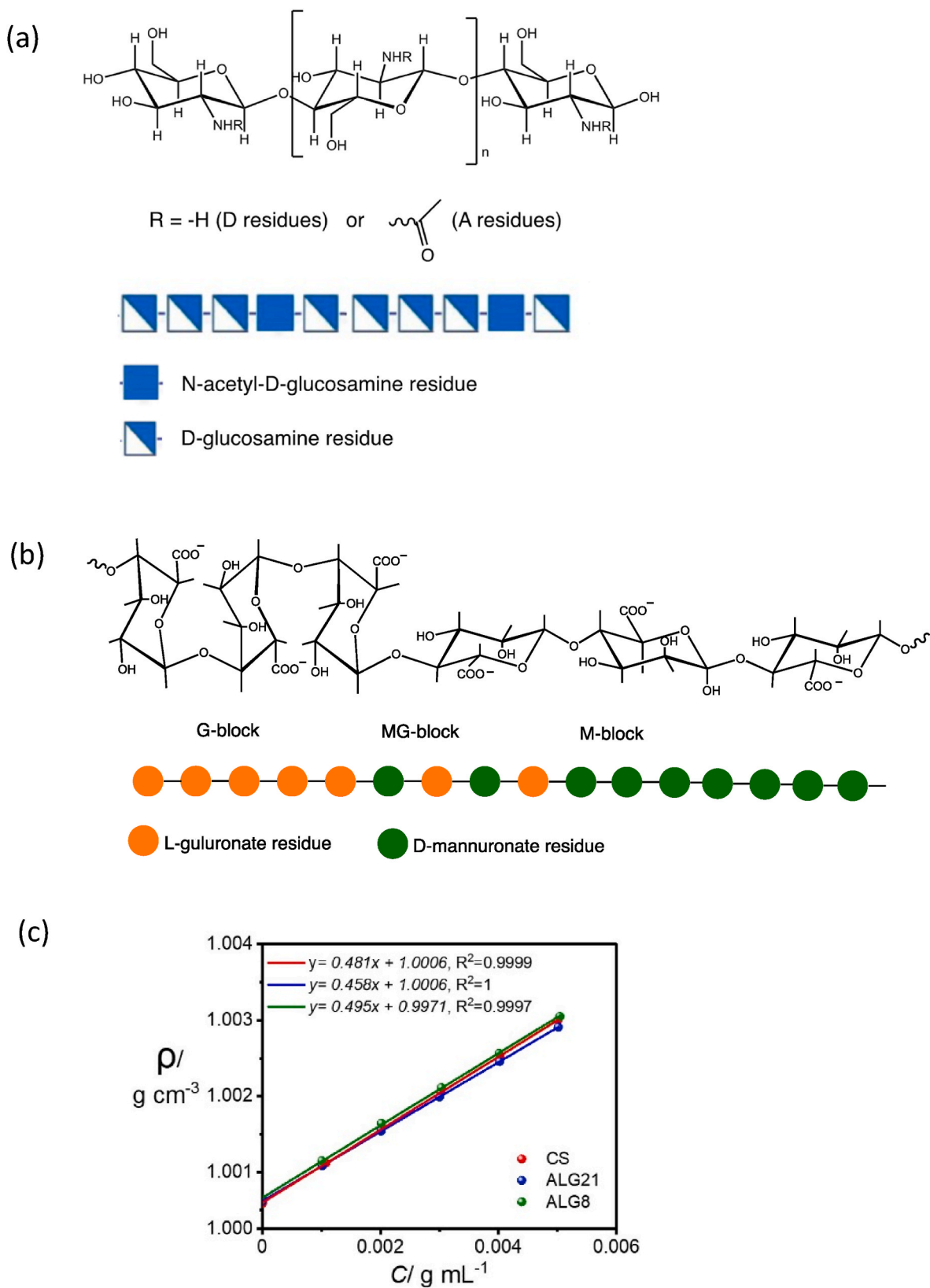
Fig. 1. (a) Chitosan (CS) and (b) alginate (ALG) schematic chemical structures, showing the constituent residues and representative sequences using the standardised symbol nomenclature for glycans (chitosan: filled blue boxes = A residues, half-filled blue boxes = D residues; alginate: orange filled circles = G residues, green filled circles = M residues). (c) Standard curves for unfiltered solution density (ρ) versus concentration (*C*): CS (red); AlG21 (blue); AlG8 (green), with the corresponding linear regression lines and coefficients shown.

PVDF syringe filter and loaded into an autosampler tube (1 mL vials). RP-HPLC was performed based on the methods of Curtis et al. (2002), Jiang et al. (2017) and Liu et al. (2020), with some modifications. A C-18 column stationary phase (Gemini®, 4.6 × 250 mm, 5 μm, 110 Å, Darmstadt, Germany) was employed. Mobile phase A was Milli-Q water, mobile phase B was ACN containing 0.05% TFA, using a flow rate of 1 mL min^{-1}. The gradient of the mobile phase for ACN was 5% (0–6 min), 15% (6–10 min), 25% (10–15 min), and 35% (15–21 min). The injection volume was 20 μL. The eluent was monitored at a wavelength (λ) = 219 nm and retention times compared with those of standard solutions of LKPNM and LKP. The solutions were stored in a refrigerator until further use.

2.3. Preparation and calibration of the CS and ALG stock solutions

CS was dissolved in 85 mM NaCl aqueous solution, to which had also been added aliquots of 12 M HCL to give 1.25x moles of H$^+$ compared to the moles of non-acetylated (ionizable) amino groups, the final CS concentration = 10 mg mL^{-1}. This NaCl concentration was found to maintain a constant particle size in CS-ALG-tripolyphosphate (TPP) nanocomplexes according to Goycoolea et al. (2009) and others for synthesizing CS-TPP nanoparticles (Milkova & Goycoolea, 2020; Sreekumar et al., 2022). The resultant pH was 4.8. ALG was dissolved in 25 mL of 85 mM NaCl to give 10 mg mL^{-1} ALG; the pH of this solution was pH 5.8. Sodium azide was added (to give 0.02% w/v) to both solutions as a preservative. Both solutions were then stirred with a magnetic stirrer overnight at 25 °C. The densities of samples of the CS and ALG solutions at a range of dilutions (0, 1.0, 2.0, 3.0, 4.0 and 5.0 mg mL^{-1}) were measured with a DMA 4500 M density meter (Anton Paar GmbH, Austria) at 25 °C and standard curves of density versus concentration for each were plotted. Measurements were carried out in triplicate. Pure water and solvent (85 mM NaCl) were initially measured to calibrate the instrument using the density of water at 25 °C (ρ = 0.997 g cm^{-3}) as a reference. All solutions were loaded into the instrument uniformly, each comprising 1 mL dispensed using a 1 mL syringe, ensuring the absence of any bubbles during the measurement. The remaining CS and ALG solutions were then filtered through a hydrophilic polyethersulfone (PES) sterile membrane (Millex®, Millipore, Ireland), pore size 0.22 μm, diameter 33 mm and their densities measured for comparison with the standard curve to obtain their final concentration (O'Connell, Goycoolea, et al., 2023). These solutions were diluted to the appropriate concentration for subsequent PEC formation, diluted with 85 mM NaCl (also previously filtered through the PES membrane). Filtration was necessary to remove any dust or large undissolved aggregated material in preparation for subsequent light scattering analysis of the solutions and their mixtures. Fig. 1 illustrates the components of the stock solutions and their density measurements.

In our preparations, CS with a M$_w$ of 111 kDa at concentrations between 0.1 and 0.5 % (w/v) exhibited ρ between 1.0012 and 1.0029 g cm^{-3}, in close agreement with the work of Kumar et al. (2021). The densities of the ALG solutions were very similar at the same concentrations (see Fig. 1), although the ALG8 gave higher ρ than ALG21 within experimental error, again in agreement with Kumar et al. (2021).

2.4. Calculation of the molar charge ratio (n$^-$/n$^+$)

On mixing, the molar charge ratio (n$^-$/n$^+$) of the polymers is given by:

$$n^- / n^+ = M_{ALG} \cdot N_{ALG}^- / M_{CS} \cdot N_{CS}^+ \qquad (1)$$

where M$_{ALG}$ = the final molar concentration of ALG, N$_{ALG}^-$ = the number of negative charges per ALG molecule, M$_{CS}$ = the final molar concentration of CS and N$_{CS}^+$ = the number of positive charges per CS molecule. N$_{ALG}^-$ and N$_{CS}^+$ are given by:

$$N_{ALG}^- = \alpha \cdot M_W ALG / M_W ALG_{mon} \qquad (2)$$

and

$$N_{CS}^+ = (1-\alpha) \cdot (1 / 100) \cdot (100\text{-}DA) \cdot M_W CS / M_W CS_{mon} \qquad (3)$$

where α is the degree of dissociation of the ionizing groups; M$_w$ALG and M$_w$CS are the M$_w$ of the ALG and CS, respectively; M$_w$ALG$_{mon}$ and M$_w$CS$_{mon}$ are the Mw of the ALG and CS monomers, respectively. DA is the % degree of acetylation of the CS. Assuming that at the pH at which the polymers are mixed both the ALG carboxylate groups and the CS amino groups are fully charged (see later), at −1 and +1, respectively, i.e., α = 1 for carboxylate and 0 for the NH$_3^+$ groups, this allows calculation of N$_{ALG}^-$ and N$_{CS}^+$ if the M$_w$ of the species are known. Taking the M$_w$ of the CS, ALG8 and ALG21 as 111, 8, and 21 kDa, respectively (as described above), plus values of 198 g mol^{-1} for ALG$_{mon}$ and for CS$_{mon}$ 166.3 g mol^{-1} (the average molar mass of the A and D CS residues, weighted according to DA = 10%) the values of N$_{CS}^+$ for CS and N$_{ALG}^-$ for ALG8 and ALG21 are 601+, 40.4− and 106−, respectively. From the known concentration (2 mg mL^{-1}, converted to M$_{ALG}$ and M$_{CS}$) of the CS and ALG stock solutions and the different volumes mixed together, n$^-$/ n$^+$ was then calculated via eq. (1).

2.5. Polyelectrolyte complex (PEC) formation

PEC preparation was carried out via a simple one step mixing technique (Goycoolea et al., 2009). The appropriate volumes and concentrations of ALG and CS solutions were mixed according to the charge ratio calculation indicated above to give a total volume = 2 mL. ALG solution was added into the CS solution via a micropipette. The mixture was then vortexed for 5 s via a Fisherbrand™ Classic Vortex Mixer (Fisher Scientific, Loughborough, UK) at room temperature (20 − 25 °C), left for 3 h then cooled to 4 °C then sonicated for 5 min (5 s pulsed ON, 3 s pulsed OFF, amplitude 35% at 20 kHz) via a Sonics® VCX 750 (Sonics & Materials, Inc., Newtown, CT, USA) ultrasonicator and tapered microtip probe. To create PECs load with BAPs, the BAP was dissolved in water then added to the CS solution before mixing with the ALG solution to give a final BAP concentration in the PECs of 1.0 mg mL^{-1}. Fig. 2 summarises the PEC preparation method.

2.6. Encapsulation efficiency (EE)

The loaded PECs were centrifuged at 20,000×g for 25 min and the free (non-encapsulated) concentration of BAP in the supernatant was determined via HPLC as described above (section 2.2). The % encapsulation efficiency (EE) was defined as:

$$100(C_i - C_s)/C_i \qquad (4)$$

(Bicak et al., 2021; Danish et al., 2017) where C_i is the initial BAP concentration in the mixture and C_s is the BAP concentration in the supernatant measured via HPLC.

2.7. Viscosity determinations

Viscosity (η) analysis of the supernatants from the PECs (both loaded and unloaded) was also performed to indicate differences in the amount of remaining, non-complexed biopolymer (Menchicchi et al., 2014), as a way of qualitatively confirming the extent of complex formation, plus these supernatant viscosities are required for accurate estimation of R$_h$ via DLS (see section 2.9). Utilizing the microVISC™ method by RheoSense, a 300 μL sample of the supernatant was loaded into the device, which is equipped with a chip featuring a rectangular slit for both inflow and outflow. The chip, enhanced with a sensory array, measures the solution's flow and viscosity as it is propelled by a plugger.
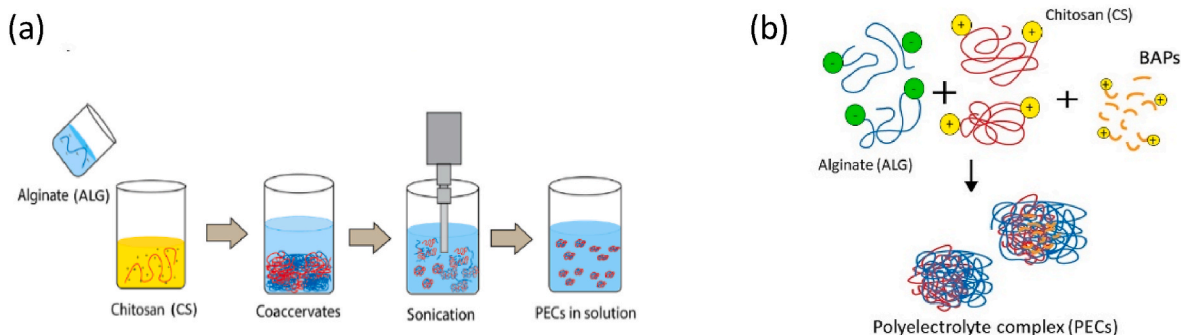
(a)

(b)

Fig. 2. (a) Schematic illustration of preparation of PECs; (b) Cartoon of complex formation with or without BAPs.

2.8. BAP release (R)

In vitro release studies were conducted at pH 3.0 and pH 6.8 based on earlier methodology (Goycoolea et al., 2009) with slight modification. After centrifuging samples of the loaded BAPs as above (section 2.6) the pellets were re-suspended in 3 mL of a mixture of 0.1 M HCl and water adjusted to pH 3 and other pellets in a mixture of water + 0.1 M NaOH adjusted to pH 6.8. The mixtures were then incubated for 3 h at 37 °C (Egger et al., 2016; Zhang et al., 2022). These two pH values and incubation times were intended to mimic the 'typical' physical gastric and intestinal conditions during human digestion of foods. After incubation, the mixtures were centrifuged at $20,000 \times g$ for 25 min then the concentration of BAP in the supernatants measured via HPLC as described above. The % release (R) was calculated as:

$$R = 100(C_{BAP} - n^-/n_S^+)/C_{BAP} \qquad (5)$$

where C_{BAP} = the concentration of BAPs in the mixture before incubation (determined by the measured EE) and $n^-/n+_S$ = the concentration of BAPs released from the mixture on incubation, measured via HPLC analysis of the supernatant.

2.9. PEC particle size measurements

The mean particle sizes, particle size distributions (PSD) and polydispersity index (PDI) were measured via dynamic light scattering (DLS). Sample suspensions were pipetted into polymethyl methacrylate (PMMA) semi-micro filling UV transparent cuvettes, path length 10 mm (VWR International, UK) then were measured in a Zetasizer Ultra (Malvern Panalytical). Measurements were performed by setting the cuvette mode on ZEN0040 and refractive index of the dispersant = 1.33 (water). Samples were equilibrated for 120 s at 25 °C and analysed using backscattered light (wavelength 633 nm) at a detection angle of 173° to determine the mean hydrodynamic radius (R_h), assuming the particles are spherical and obey the Stokes-Einstein eq.:

$$R_h = \frac{k_B T}{3 \pi \eta D} \qquad (6)$$

where, k_B is Boltzmann's constant, T is absolute temperature (298.15 K) and D is diffusion coefficient as measured by the instrument (Anderson et al., 2013; Stetefeld et al., 2016). The ζ-potential of the particles was calculated from their electrophoretic mobility (μ) measured by mixed-mode phase analysis light scattering (M3-PALS). Samples were diluted 50x (100 μL of sample to 5 mL of 10 mM NaCl at pH ∼ 7) and vortexed. (This NaCl concentration was to fix the ionic strength, but at a low value in order to avoid particle aggregation or complex dissolution). Then 0.8 mL of sample was loaded into a folded capillary zeta cell DTS1070 and subsequently measured via a Zetasizer Ultra (Malvern Panalytical) equipped with a 4 mW He/Ne laser beam (λ = 633 nm) at 25 °C. The zeta potential (ζ) was calculated via the Smoluchowski approximation:

$$\zeta = \frac{4\pi \eta \mu}{\varepsilon . \varepsilon_0} \qquad (7)$$

where ε_r is the relative dielectric constant of the solvent (for water and 10 mM NaCl ≈ 78.5), ε_0 the permittivity of free space 8.854×10^{-12} F m^{-1}) and $\mu = \nu/E$, where ν is measured particle velocity in an electric field of strength E (Doroszkowski, 1999; S. Zhang, Murray, et al., 2021). Some samples of both loaded and unloaded PECs were transferred into an Eppendorf tube containing a small amount of glycerol then centrifuged at $20,000 \times g$ for 25 min. The supernatant was discarded, and the pellet re-suspended in filtered 85 mM NaCl and mixed via a micropipette for re-examination of PEC particle size.

2.10. Small angle X-ray scattering (SAXS)

Small angle X-ray scattering (SAXS) was conducted on unloaded PECs at 25 °C. SAXS measurements were performed utilizing a SAXSpace small-angle X-ray camera Anton Paar (Graz, Austria). Briefly, the X-ray beam was collimated into a line focus, length = 20 mm and width = 0.5 mm. The distance of sample to detector was 317 mm, determined via utilization of silver behenate powder. Each sample was loaded into a 1.5 mm diameter quartz capillary tube and exposed for 3600 s to a beam from an X-ray tube (wavelength 0.154 nm) operating at 40 kV and 50 mA. The instrument system was additionally run in high-intensity mode, offering a minimum accessible scattering vector magnitude $q_{min} = 0.12$ nm^{-1} (where $q = 4\pi/\lambda \sin(\theta)$, and 2θ represents the scattering angle). Further details of the instrument and its operation are available elsewhere (Apostolidis et al., 2023).

2.11. Electron microscopy (EM)

Transmission electron microscopy (TEM) was performed to observe the size and morphology of selected loaded PECs. The liquid sample was pipetted onto a copper TEM grid placed on filter paper, then allowed to dry under cover. The grid was then placed carefully into a TEM specimen holder via tweezers and the grid clamped. TEM analysis was carried out using a FEI Titan3 Themis G2 S/TEM (Massachusetts, USA) operated at 300 kV with an energy spread ≈ 0.25 eV and fitted with Gatan OneView 4K CMOS digital camera.

2.12. Statistical analysis

The data outcomes have been presented as mean values and their associated standard deviations of 3 repeat measurements, except for the HPLC measurements, which were only repeated twice. SPSS Statistics 29.0 (IBM, Chicago, IL) was employed for the data analysis. The efficacy of the treatment was assessed through a one-way analysis of variance (ANOVA), followed by the application of Tukey's test. Statistical significance was established at a threshold of $p < 0.05$.

3. Results and discussion

3.1. BAP fractionation and identification

The HPLC chromatograms (Fig. 3) revealed two predominant peptides in the ultrafiltrate of the PeptACE sample, characterized by high-intensity and sharp peaks at retention times between 105–117 and 218–225 s. These peaks coincided with those of the two synthetic peptides LKP and LKPNM when introduced under the same conditions at concentrations ranging between 0.05 and 0.25 mM. This agrees with previous studies (Curtis et al., 2002; Fuentea et al., 2020; Fujita & Yoshikawa, 1999). The LKP eluted just before LKPNM, probably owing to its lower M_w and higher solubility in the hydrophilic mobile phase.

The existence of LKP may stem from the hydrolysis of LKPNM, as indicated earlier (Fujita et al., 2000; Fujita & Yoshikawa, 1999) where it was shown that LKPNM yielded two peptides: LKP and NM. Notably, LKP exhibited an eight-fold higher antihypertensive activity than the original LKPNM, with an IC_{50} of 0.32 μM, whilst NM did not manifest any bioactivity. No additional BAPs were observed, despite assertions claiming the presence of six short fish peptides (Guan et al., 2001). A study conducted by Curtis et al. (2002) reported that the BAPs in the PeptACE® exhibited 95% similarity with synthetic LKPNM, via LC-MS analysis. PeptACE® is supposed to contain 85% peptides with an IC_{50} of 50.2 μg mL^{-1} (2.40 μM). It is pertinent to mention that LKPNM is completely soluble in water, possessing an isoelectric point ranging from 9.6 to 10.5 (Curtis et al., 2002; Fujita & Yoshikawa, 1999).

Fig. 4 shows theoretical plots of the net charge on the peptides, chitosan and the alginates as a function of pH, taking into account the varying values of α based on the pKa values of the various ionizing groups (α = (K_a/([H$^+$] + K_a))). The pKa values for the α-NH$_2$, LYS side-chain NH$_2$ and terminal COOH group of the peptides (LKPNM or LKP) were taken as 9.3, 10.2 and 2.2, respectively (Belitz & Grosch, 1999). The pK$_o$ value of the CS NH$_2$ groups was taken as 6.0 (see above) and the alginate mannuronic and guluronic COOH groups 3.38 and 3.65, respectively (see earlier). The number of NH$_2$ and COOH groups on the CS and ALG molecules were calculated as described above, plus, in the case of the alginates, also the M/G ratio to calculate the average number of Man*p*A and Gul*p*A residues per molecule of ALG21 and ALG8. It is
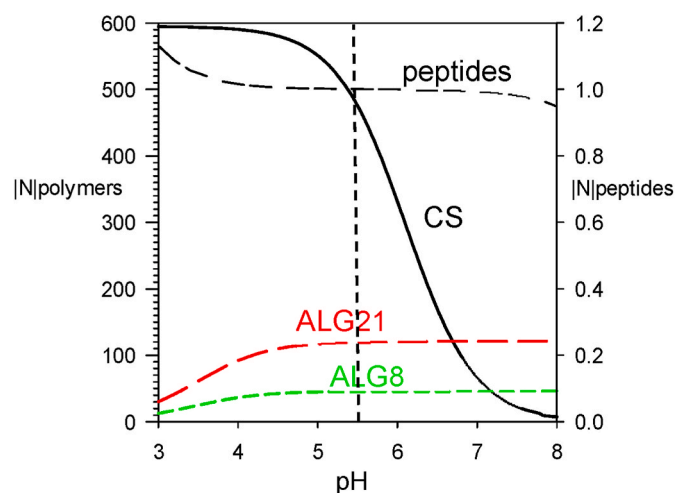

Fig. 4. The magnitude of the net charge |N| on single molecules of the polymers and the BAPs as a function of pH. Left hand ordinate: |N| (+ve) for CS (full black line); |N| (-ve) for ALG21 (red long dashed line); |N| (-ve) for ALG8 (green short dashed line). Right hand ordinate: |N| for the LKPNM or LKP peptides. (Calculation explained in the text). The vertical dashed line indicates the pH (5.5) of PEC formation.

seen that at the pH of PEC formation (5.5) the charge on the CS is dominant, approximately 4 and 11x as large (and opposite in sign) to that on the ALG21 and ALG8 molecules, respectively. The net charge (~+1) on both BAPs is minuscule in comparison, but because of their lower M_w, the molar concentration of +ve charges due to the BAPs becomes significant, as will be explained below. Between pH 3.0 and 5.5 CS loses approximately 20% of its full charge; by pH 8 CS would have lost almost all its charge. Decreasing the pH from 5.5 to pH 3.0 results in the ALG losing approximately 70% of their –ve charge.

3.2. Physical properties of unloaded CS + ALG PECs

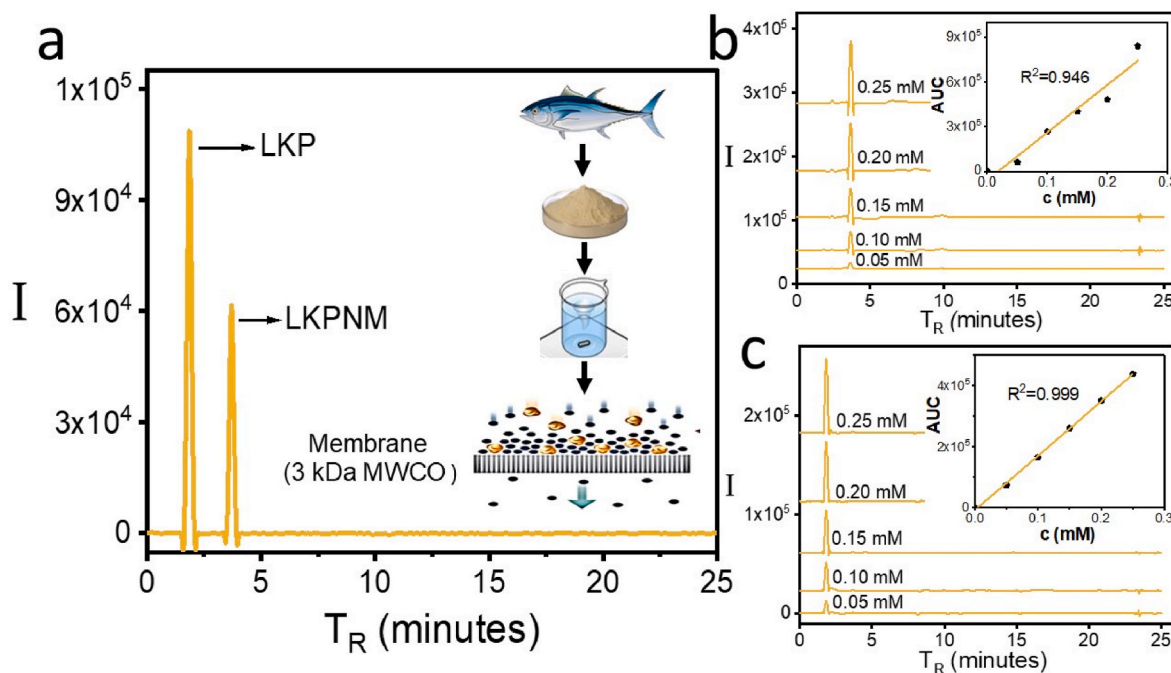Fig. 5 shows the measured hydrodynamic radius (R_h) and

Fig. 3. (a) HPLC chromatograms of ≤ 3 kDa PeptACE BAPs and their fractionation scheme. Standard curves for LKPNM (b) and LKP (c) calculated from area under the curves (AUC).
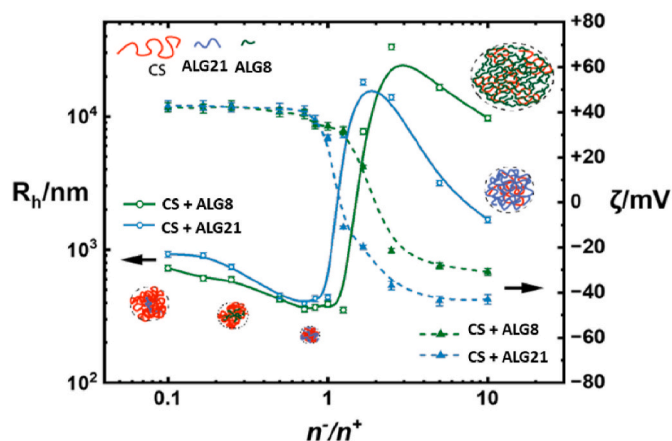
Fig. 5. Hydrodynamic radius (R_h) and ζ-potential of unloaded PECs as a function of molar charge ratio n^-/n^+ at a total polymer concentration of 2 mg mL^{-1}.

ζ−potential of PECs formed (in the absence of added BAPs) as a function of the molar charge ratio n^-/n^+, between $n^-/n^+ = 0.1$ (excess CS) and $n^-/n^+ = 10$ (excess ALG) for CS + ALG21 and CS + ALG8. (Note that these R_h values were calculated taking into account the viscosity of the background solutions, measured when the PECs were centrifuged off – see Fig. 7 below, whereas the samples were highly diluted into water for the ζ measurements). n^-/n^+ is generally a critical parameter influencing the formation and stability of such PECs, whilst there seems to be a scarcity of work focusing on this. To the best of our knowledge, only few studies such as the ones conducted by Becheran-Maron et al. (2004), Sæther et al. (2008) and Yilmaz et al. (2019) have endeavoured to control the n^-/n^+ in CS + ALG PECs formation. Conductometric and potentiometric titrations, along with turbidity measurements in CS + ALG PECs, revealed that the full charge neutralisation occurs at a non-stoichiometric n^+/n^- − charge ratio of 0.70 ± 0.2 (i.e., $n^-/n^+ \sim 1.43$), thus reflecting the pivotal role of the weak electrolyte character and nature of the polymers (Becheran-Maron et al., 2004). Meanwhile, the other two studies concurred that as n^-/n^+ approaches 1 the electrostatic attraction intensifies, leading to the formation of coacervates or larger aggregates. This is seen for both CS + ALG systems, where a large increase in R_h occurs around $n^-/n^+ = 1$. At the same time, this coincides with a change in the sign of the ζ, from positive to negative. For $n^-/n^+ > 1$, R_h decreases again, whilst the ζ values tend to level off – at −30 and −42 mV for the ALG8 and ALG 21 systems, respectively. For $n^-/n^+ < 1$ R_h of the PECs is much smaller and decreases a little (from ca. 800 to 300 ± 50 nm) as $n^-/n^+ 1 \to 1$, with the ALG8 + CS system giving lower R_h than the ALG21 + CS system, within experimental error, whereas the ζ-potentials of the two systems are indistinguishable. Between $n^-/n^+ = 0.1$ and 1 R_h are <1 μm but for $n^-/n^+ > 1$, where the charge inversion occurs, all $R_h > 1$ μm, especially just beyond $n^-/n^+ = 1$, suggesting that much less compact PEC structures are formed in the presence of excess ALG. Note the polydispersity of the sizes is also larger at the higher values of n^-/n^+. This is in agreement with the findings of Yilmaz et al. (2019), who reported smaller R_h when CS was in excess rather than ALG. Also notable is that the range of n^-/n^+ where the charge inversion and steep rise in R_h occur for $n^-/n^+ > 1$ is displaced to higher n^-/n^+ in the case of the lower M_w ALG8. The final R_h (at $n^-/n^+ = 10$) for the CS + ALG8 system is also considerably higher than for the CS + ALG21 system: these final values being approximately 10 and 2 μm, respectively. Thus, the lower M_w ALG when in excess ($n^-/n^+ > 1$), appears to give more expanded and lower charged PECs than those formed with the higher M_w ALG, perhaps indicating that the ALG8 is less 'efficient' than ALG21 in being able to pull CS chains together to form the PECs at the same n^-/n^+. Note that there will be more molecules of ALG8 than ALG 21 available at the same n^-/n^+, but if the cross-linking between the two

types of polymer is a co-operative process depending upon multiple points of attraction between the different polymers, then it makes sense that the higher M_w ALG is more efficient as an agent of cross-linking.

According to Vold et al. (2006) the persistence length of ALG, at 12 nm, tends to be larger than that of this type of CS: ca. 5 nm (Rinaudo et al., 1993; Schatz et al., 2004). In other words, ALG is stiffer than CS, so that, even though the CS M_w is so much higher, ALG might be expected to have a disproportionate effect on the size of the complexes of the two molecules.

Fig. 6 compares the values of R_h determined via DLS with the radius of gyration (R_g) as determined by SLS (at scattering angles between 30 and 130°) for freshly prepared PECs at $n^-/n^+ = 0.5$ and 10 for CS + ALG21.

For the PEC particles formed at these ratios, we applied the spherical particles scattering model to fit the angular dependency of scattered intensities from SLS data. The analysis provided us with asymmetric size distributions for different PECs with a skewness towards large dimensions and the average radius of gyration (R_g) for each sample. (SLS data fitting and size distributions are reported in Fig SI1). It is interesting that the R_g values are considerably and consistently lower than R_h for both n^-/n^+. This probably indicates that the core of the structures in both cases is somewhat similar, whilst the outer layers differ – R_h being much more sensitive to the presence of long, less dense 'hairy' layers at the surface. Thus, the smaller difference between R_h and R_g in the case of $n^-/n^+ = 0.5$ again points to these particles having a more compact structure – when CS is in excess rather than ALG in excess ($n^-/n^+ = 10$). Typical reported R_g: R_h ratios for spherical nanoparticles are 0.775 and for macromolecules between 1 and 2; ratios >2 generally indicate anisotropy in the molecules, i.e., elongated conformations such as rod-like conformations. Ratios <0.7 typically represent highly swollen macromolecules or "micro gels" (Schmidt et al., 1979). Using macromolecular fractionation techniques, such as asymmetric flow field-flow fractionation (AF4) coupled to SLS and DLS detection, the determination of R_g: R_h ratios also allows one to distinguish between aggregated and non-aggregated structures in a population (Glantz et al., 2010; Hakansson et al., 2012; Nilsson, 2013). (Also notable is that the R_h values are lower when the system is loaded with BAP – this is discussed later in section 3.3).

The more efficient cross-linking via ALG21 discussed above (Fig. 5) is also hinted at by the results in Fig. 7a and b, which show the viscosities (η) of the supernatants when centrifuging off the PECs, as a function of the mass fraction (f) of ALG in system. A measured viscosity (η) further away (lower) than the theoretical additive line (which assumes no
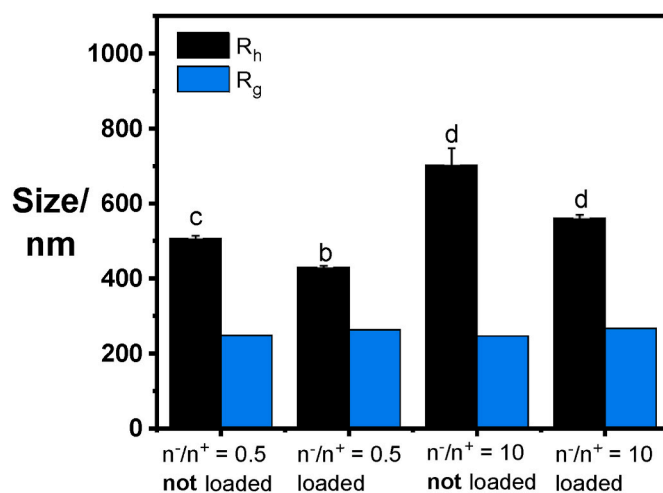

Fig. 6. Measured PEC sizes via *DLS* (R_h, black) and *SLS* (R_g, blue) for the CS + ALG21 systems at $n^-/n^+ = 0.5$ and 10, both loaded and unloaded with BAPs. (Bars with different letters are values that are statistically different from one another, at $p < 0.05$).
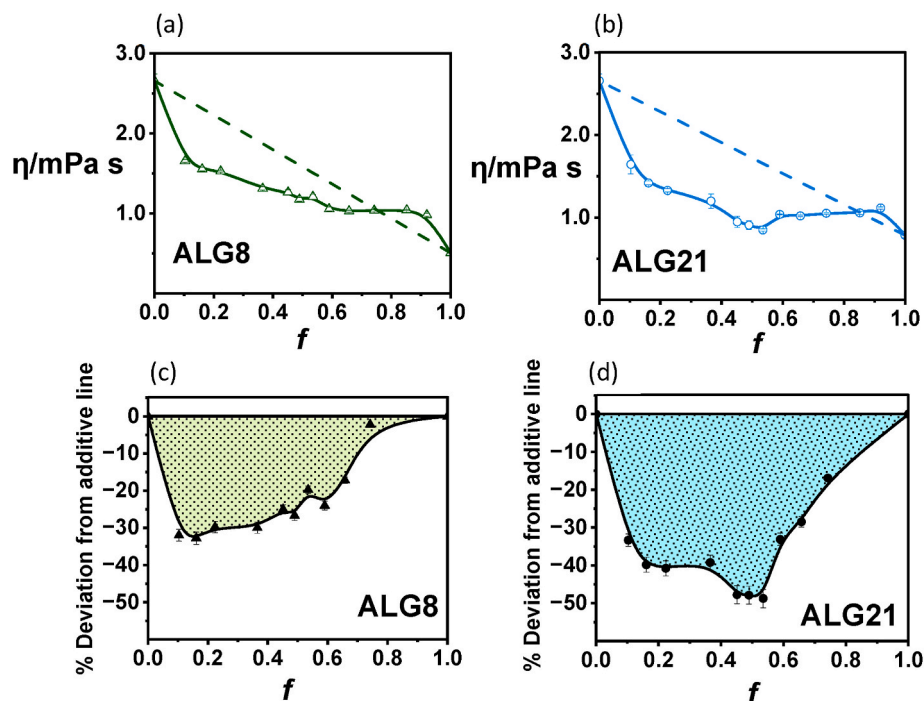
Fig. 7. Viscosity (η) of the supernatants of centrifuged CS + ALG mixtures as a function of the original mass fraction of ALG (*f*) in the systems for (a) CS + ALG8 and (b) CS + ALG21 at 25 °C. The dashed lines in (a) and (b) are the theoretical η of the biopolymer mixtures assuming simple additivity of the η of the pure components. (Thus η at *f* = 0 and 1 are the values of CS and ALG stock solutions at 2 mg mL^{-1}, respectively). Figures (c) and (d) show the % difference of the measured η from the additive line for CS + ALG8 and CS + ALG21, respectively.
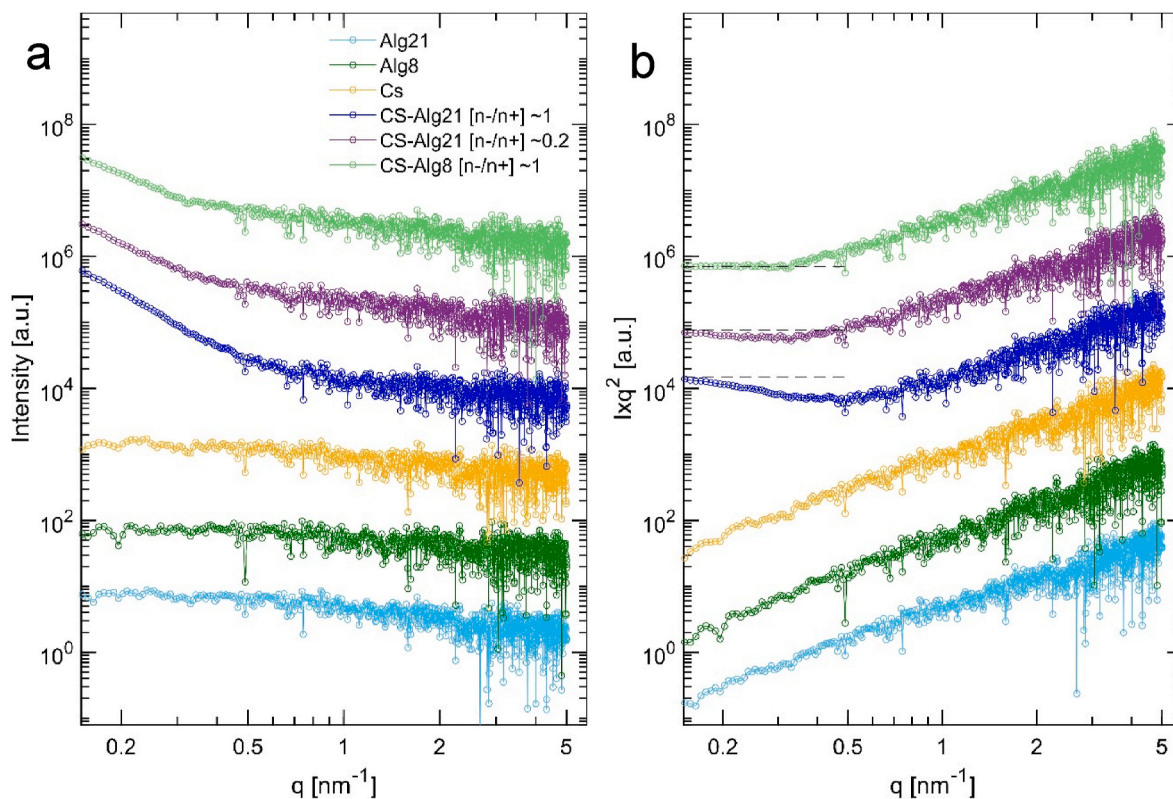

Fig. 8. Small-angle X-ray scattering (SAXS) patterns (a) and corresponding Kratky plots (b) are presented for 2 mg mL^{-1} CS, ALG, and their PECs at two different n$^-$/n$^+$ molar charge ratios. The Kratky plots demonstrate swollen chain behaviour for pure polyelectrolytes, whereas Gaussian and collapsed chains/clustered structures are observed for PECs of ALG8 and ALG21, respectively. The scattering profiles were acquired at 85 mM NaCl and 25 °C. The horizontal dashed lines in the Kratky plots provide a guide for the Gaussian (random coil) chain behaviour at low q values.

interaction between the polymers in dilute solution) indicates that higher levels of polymer have become trapped within the PECs. The same dilute solution viscosity method was used in previous studies to determine the degree of interaction between chitosan and other polysaccharides with soluble mucin (Menchicchi et al., 2014, 2015), and between polysaccharides of varying structure and conformation (Goycoolea-Valencia et al., 1995). It is seen that η is overall closer to the additive line in the case of the CS + ALG8 system (Fig. 7a). Quantitatively the integrated area between the curve describing the data points and the additive straight line is larger (1.7 x larger) for CS + ALG21 than CS + ALG8 (see Fig. 7(c) and (d)). For CS + ALG8 between f = 0.7 and 1, η was higher than the theoretical additive line, which might be due simply to the limits of sensitivity of the measurement at these low η, or due to non-homogeneous mixing or incomplete separation of components during centrifugation, since the η of the ALG8 stock solution was considerably lower than that of the CS, so that relatively minor variations in CS content will have a disproportionately large effect on the overall η. Similarly, this condition also occurs in the CS + ALG21 systems at $f > 0.92$.

Fig. 8 shows the SAXS patterns (Fig. 8a) and corresponding Kratky plots (Fig. 8b) before and after complexation. Intensities in Y-axis of both curves are shown in arbitrary units and shifted vertically for the sake of clarity. For pure CS and ALG polyelectrolyte solutions, scattering intensities (I) demonstrate a slow decay by scattering vectors (q) which is accompanied by a monotonous increase of $I \times q^2$ in the Kratky plot. The behaviour indicates the existence of homogeneous solutions of stretched chains of polyelectrolytes. The stretching is enforced by the high charge along the biopolymer chains at the pH condition studied. In contrast, after mixing the two biopolymers and upon formation of PECs, a much higher angular dependency is observed (the intensity versus q decays faster compared to the pure polyelectrolytes). The intensities decay considerably until q = 0.5 nm^{-1} (associated with the length scale >12 nm), however, the rate of these decays is dependent on the type and molecular weight of polyelectrolytes. To understand the chain arrangement for different PECs, a close look into Kratky plots is helpful. For the PEC of ALG8 at n$^-$/n$^+$ = 1, the Kratky plot shows a plateau at low q, confirming a Gaussian chain (random coil) behaviour (Takeshita et al., 2019). The dashed lines in Fig. 8b represent the Kratky plot behaviour of ideal Gaussian chains. The line is perfectly aligned with the experimental data for CS + ALG8 PEC at n$^-$/n$^+$ = 1. In contrast, the complexes of ALG21 at both ratios (n$^-$/n$^+$ = 1 and n$^-$/n$^+$ = 0.2) show decreases in $I \times q^2$ versus q at q < 0.5 nm^{-1}. This deviation from Gaussian chain behaviour indicates more collapsed chain configurations and possibly the formation of larger clusters in PEC samples. The deviation is more pronounced in the case of CS + ALG8 PEC at n$^-$/n$^+$ = 1 (see blue curve in Fig. 8b). It is noteworthy that all SAXS curves behave similarly at higher q values (q > 0.5 nm^{-1}), indicating that the chains appear swollen when focusing on very small length scales (length scales below 12 nm).

3.3. Physical properties of loaded CS + ALG PECs

In view of the sensitivity of the properties of the unloaded PECs to n$^-$/n$^+$, particularly around n$^-$/n$^+$ = 1, two extremes, n$^-$/n$^+$ = 0.5 and 10 for ALG 21, were chosen to test the effects of addition of BAPs to the systems and their loading. In addition, of course, these two extremes are predicted to form complexes of very different sizes (assuming the same behaviour as in Fig. 5), i.e., sub-micron and >1 μm, which might have different release properties and applications, whilst their higher ζ values are likely to prevent them aggregating. LKPNM and LKP from the ultrafiltration of fish peptides were encapsulated into PECs as described in the Methods, adding the BAPs to the CS solution before mixing with ALG. Thus, the starting solution contained *two* net positively charged molecules, the CS *and* the BAPs. The results are shown in Table 1.

It is seen that both for n$^-$/n$^+$ = 0.5 and 10, including the BAPs

Table 1

Comparison of measured properties of CS + ALG21 PECs with and without BAP loading. n$^-$/n$^+$ = molar charge ratio; R$_h$ hydrodynamic radius; PDI = polydispersity index; ζ = zeta potential; EE = encapsulation efficiency.

System	n$^-$/n$^+$	R$_h$/nm	PDI	ζ/mV	EE/%	PEC yield /%
no BAPs	0.5	402 ± 13 [a]	0.25 ± 0.02 [a]	+36.0 ± 2.1 [a]	–	8.6 ± 0.7[bc]
with BAPs	0.5	322 ± 2 [a]	0.19 ± 0.01 [a]	+33.9 ± 1.3 [b]	85 ± 0.1	13.5 ± 1.1[ab]
no BAPs	10	843 ± 88[b]	0.49 ± 0.06 [b]	−23.0 ± 1.3 [c]	–	3.0 ± 1.4[c]
with BAPs	10	436 ± 54[a]	0.42 ± 0.04 [b]	−14.6 ± 2.3[d]	80.6 ± 0.5	6.9 ± 5.8[bc]

Symbols in the same column with different notations indicate differences with significance >95% (p < 0.05).

resulted in a significant reduction in R$_h$ and PDI (as already noted in Fig. 6), suggesting that the BAP contributed to the cross-linking and led to more compact structures. A PDI value between 0 and 0.1 indicates monodispersity (Raval et al., 2019), between 0.1 and 0.3 suggests moderate polydispersity but still relatively uniform (Gazzillo et al., 2006) whereas PDI values between 0.3 and 1.0, or greater than 0.7, signify a diverse range of particle sizes (Mudalige et al., 2019). The yield of PECs also increased significantly when the PECs were formed in the presence of the BAPs, reinforcing the supposition that the BAPs contributed to PEC formation. At the same time, it is noticeable that with the BAP included the value of ζ attained was smaller in magnitude: less + ve for n$^-$/n$^+$ = 0.5 (excess CS) and less -ve for n$^-$/n$^+$ = 10 (excess ALG). In the latter case, this might indicate that the BAP has more of an effect on the cross-linking at the surface of the PEC, whereas with excess CS the CS dominates over any structural effect due to the BAP. Similar increases in the yields of PEC formation (>∼50%) were observed in CS + ALG nanoparticles comprising low M$_w$ alginate upon loading them
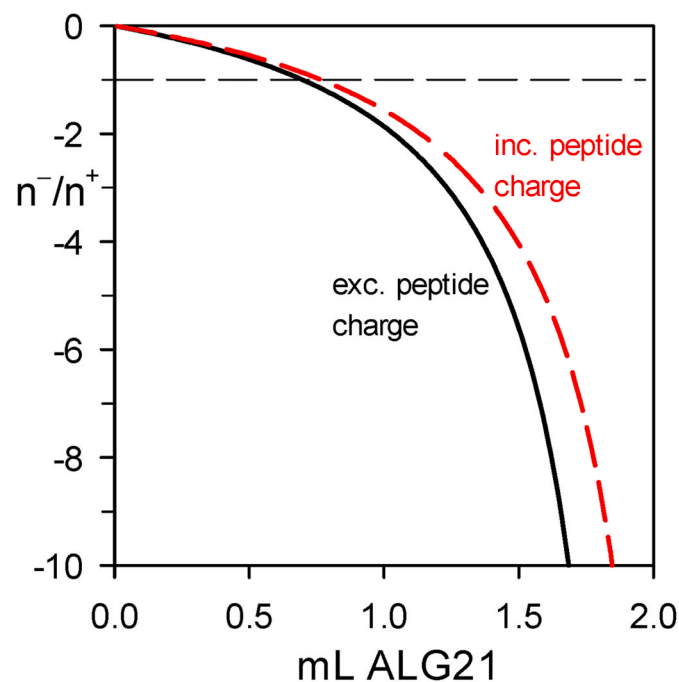

Fig. 9. The signed molar charge ratio −(n$^-$/n$^+$) for the CS + ALG21 PECs calculated excluding (black full curve) and including (red dashed curve) the contribution of charges from encapsulated BAPs as a function of the volume of 2 mg mL^{-1} stock ALG21 solution added into the system. The horizontal dashed line indicates n$^-$/n$^+$ = 1, i.e., overall charge compensation of the systems.

with insulin (Goycoolea et al., 2009).

Fig. 9 shows the molar charge ratio of –ve species (ALG21) to +ve charged species when the moles of charge carried by the encapsulated BAPs are included, compared to when the latter is ignored (as in Fig. 5). (In this case, we have given the ratio the appropriate sign to indicate whether the net charge is negative or positive). Even though there is only one net +ve charge per BAP molecule, compared to 601 per CS molecule, it is seen that the contribution of the BAPs to the n^-/n^+ does become significant as $n^-/n^+ \rightarrow 10$, i.e., in the ALG21-rich but CS-depleted complexes, due to the much higher molar concentration of the BAPs. This adds further weight to the hypothesis that in the latter systems the BAPs themselves may contribute to the structure and integrity of the PECs formed.

The encapsulation efficiency was similar and high for both systems −85 % for $n^-/n^+ = 0.5$ and 80.6 % for n^-/n^+ 10 − therefore just higher (within experimental error) for the more compact PECs. Danish et al. (2017) reported EE between 22.6% and 43.9% for the encapsulation of the tripeptide IPP and 40.9%–65.1% for the encapsulation of LKP into CS nanoparticles (NPs). The EE of tripeptide YKT into CS 'macro-particles' (MP) was approximately 35% (Bicak et al., 2021). Encapsulation of the decapeptide YLGYLEQLLR into guar gum coated with CS MPs yielded an EE of about 86%. The CS + ALG system reported in this work therefore seems at least as good if not better than these other systems reported.

We also investigated the influence of re-suspension of CS + ALG21 PECs, both loaded and unloaded, on their R_h, ζ-potential and PDI to check for their stability to re-dispersal and dilution after their isolation. The results are shown in Fig. 10, expressed as the ratio of the values for the fresh to re-suspended. For $n^-/n^+ = 0.5$ (excess CS) the ratios were close to 1, indicating no significant differences. However, for $n^-/n^+ = 10$ (excess ALG) the ratios were significantly >1, particularly for the R_h and ζ values, indicating that the PECs with excess ALG were less stable, noting that these PECs were much larger and therefore possibly less compact to start with. This was further corroborated by comparing η of the supernatants after centrifugation. The results are shown in Fig. 11 and indeed indicate that η was lower for the loaded PECs, indicating a greater proportion of the polymer being incorporated into the PECs when BAPs were present, but especially when CS was present in excess.

3.4. Microscopy evidence of PEC morphology

The morphology of the smaller PECs with the highest BAP loading (i.e., excess CS, at $n^-/n^+ = 0.5$ with ALG21) was examined via transmission electron microscopy (TEM) – see Fig. 12. The size as measured
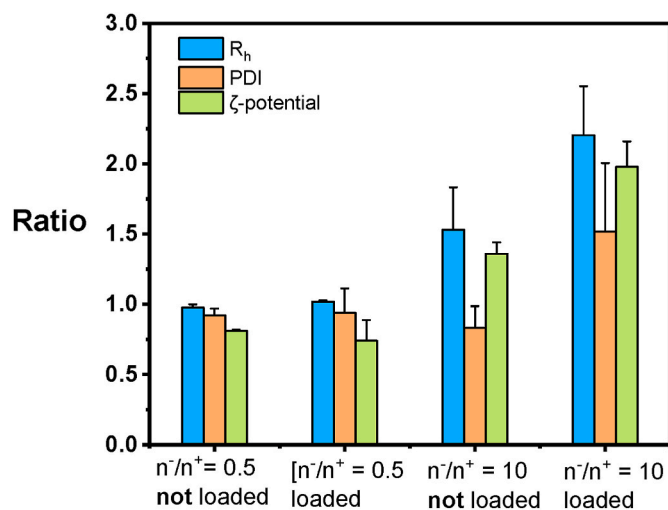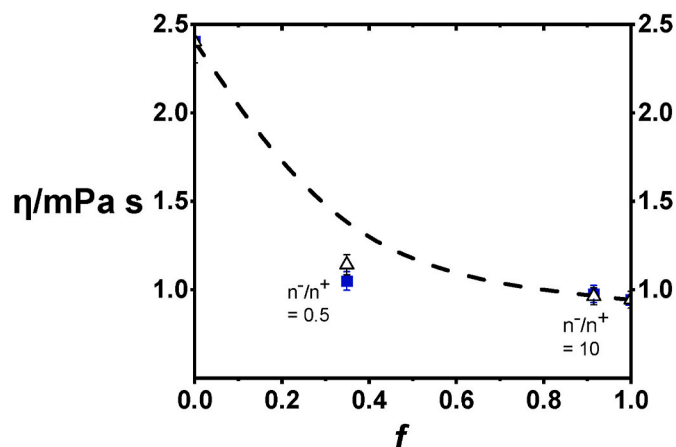

Fig. 11. Viscosity (η) at 25 °C of the supernatants of centrifuged CS + ALG21 mixtures as a function of the original mass fraction of ALG21 (*f*) in the system. The dashed curve represents the data for the unloaded system, taken from Fig. 7b. The blue filled squares indicate the η values for the PECs loaded with BAPs, the open triangles the unloaded (but re-suspended) PECs.

via DLS was approximately 322 nm whereas the TEM images showed particles ranging from less than 20 nm to over 500 nm, with some larger particles exceeding 1 μm. Some of these structures appeared to consist of aggregates. Within these structures smaller objects (<20 nm) were consistently observed, which also seemed to form larger clusters in some regions. It cannot be certain, but these smaller objects were presumed to be aggregates of the encapsulated BAP. This is in overall agreement with the low R_g: R_h ratios discussed above (Fig. 5), and future fractionation studies using asymmetric flow field-flow fractionation could shed more light on the presence of aggregates, as shown in previous studies focused on polysaccharide and protein systems (Glantz et al., 2010; Hakansson et al., 2012; Nilsson, 2013; O'Connell, Gonzalez-Espinosa, et al., 2023). Most other microscopic observations of PEC-type structures with encapsulated peptides suggest spherical-like PEC structures are formed (Chen et al., 2017; Huang et al., 2017; Jiang et al., 2021). Huang et al. (2017) focused on pentapeptide VLPVP-loaded sodium ALG-O-carboxymethyl CS microspheres and noted that the surface of the microspheres appeared rough when peptides were included, though it is not clear if this roughness was due to the sort of proposed BAP aggregates as observed in Fig. 12. We attempted SEM measurements on the samples, but unfortunately, these were very inconclusive, due to the drying out of the samples, that induced dense aggregation of the particles.

4. Studies of BAP release from PECs

As an initial study into BAP release from the type of PECs described above, we first chose to check the effect of pH and salt, i.e., without including digestive enzymes. Although such enzymes are not expected to digest the ALG or CS, they may have effects on the BAPs, which as we have shown to seem to also affect the PEC structure when encapsulated at this level. At the same time, it is well known that pH and salt will affect the electrostatic interactions thought to be holding the PECs together, so it seemed important to try and separate out the effects of enzymes and pH/salt in the first instance.

The CS + ALG21 PECs for $n^-/n^+ = 0.5$ (excess CS) and $n^-/n^+ = 10$ (excess ALG21) were incubated for 3 h at 37 °C at pH 3 (representative of gastric pH) and at pH 6.8 (representative of intestinal pH), in separate experiments. These two pH values and incubation times were intended to mimic 'typical' physical gastric and intestinal conditions during human digestion of foods (Egger et al., 2016; Zhang et al., 2022). The suspensions were then centrifuged and the amounts of BAPs released in the supernatants were quantified via RP-HPLC in the way already

Fig. 10. Ratio between freshly prepared and re-suspended values of R_h, PDI and ζ of both loaded and unloaded CS + ALG21 PECs, at $n^-/n^+ = 0.5$ and 10.
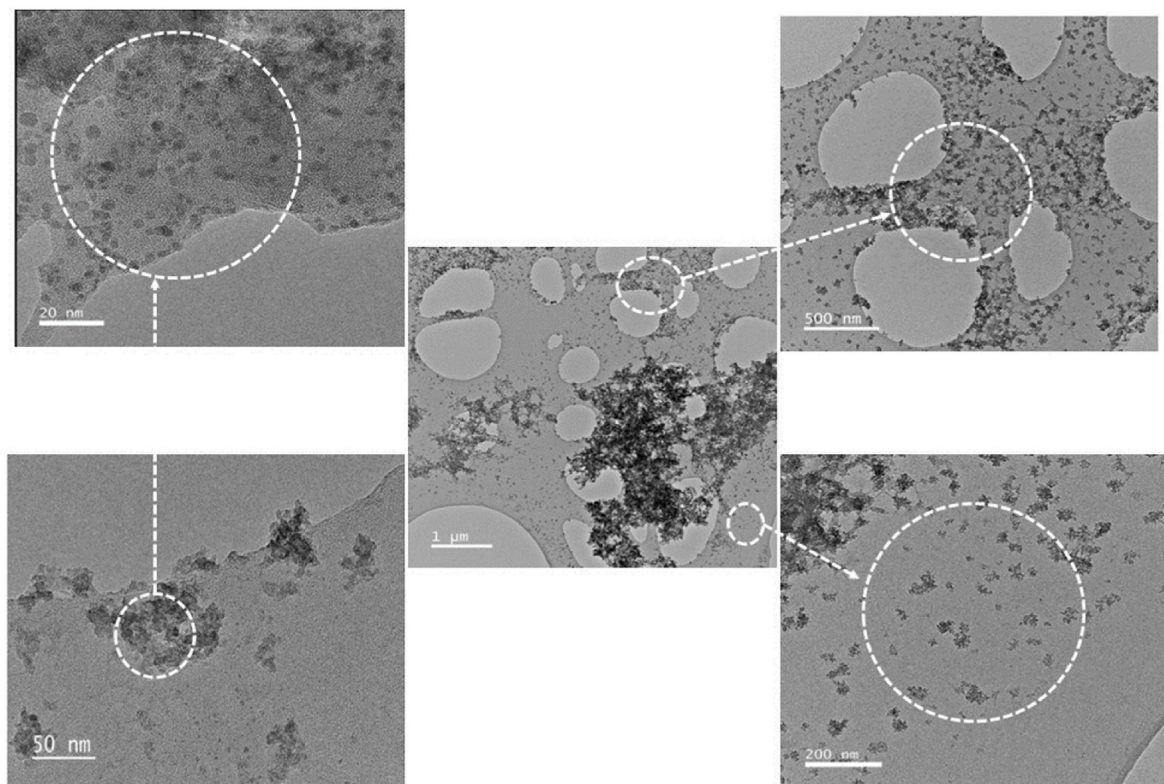
Fig. 12. TEM micrographs of PECs loaded BAPs for CS + ALG21 at $n^-/n^+ = 0.5$.
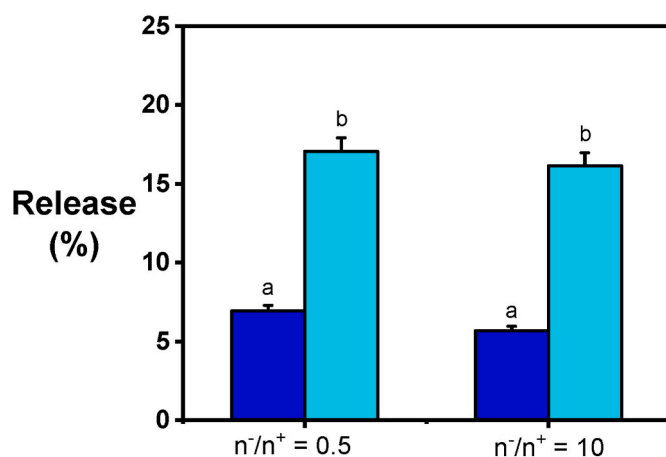

Fig. 13. The % release of BAPs from CS + ALG21 PECs for $n^-/n^+ = 0.5$ (excess CS) and $n^-/n^+ = 10$ (excess ALG21) after 3 h at 37 °C at pH 3.0 (blue) and pH 6.8 (cyan). (Bars with different letters are values that are statistically different from one another at $p < 0.05$).

described. The results (Fig. 13) showed that BAP release was less than 8% at pH 3 and less than 18% at pH 6.8. The higher release at pH 6.8 is probably due to the charge states of the CS, ALG and BAPs. At pH 3 both the CS and the BAP carry significantly higher positive charge than at pH 6.8 (see Fig. 4), leading to stronger attractive interactions with the ALG, which is expected to hold the oppositely charged polymers more closely together in the PECs, possibly with smaller pore size, reducing any diffusive loss of BAP. At the same time, the BAP itself will be more strongly bound to the ALG chains within the PEC structure.

Comparing with other previous studies, the release of short-chain BAPs during simulated gastrointestinal digestion is a common observation across a range of carrier systems, though the release kinetics tend to be mitigated when utilizing composite or hybrid wall materials, as observed in our case. For instance, the tripeptide ECG loaded into CS/β-cyclodextrin (β-CD) nanoparticles exhibited 100% and 25% release after 200 min incubation at pH 1.2 and 6.8, respectively. A similar tri-peptide loaded into CS/α-cyclodextrin (α-CD) showed 60% release after 200 min and 100% release from CS/SBE-β-cyclodextrin after 100 min (Trapani et al., 2010) where SBE = sulfobutylether moieties attached to the β-cyclodextrin. When the dipeptide FW was loaded into whey microbeads, the release = 56% after 6 h incubation of 20 % volume fraction of microbeads in deionized water (O'Neill et al., 2015). Additionally, the pentapeptide VLPVP encapsulated within O-carboxymethyl CS/sodium ALG microspheres gave 9.59 % release at pH 1.2 after 2 h and 87.63 % release at pH 6.8 after 5h (Huang et al., 2017). Guar film-coated CS microparticles gave very good protection against release of the decapeptide YLGYLEQLLR in artificial saliva (pH 6.8), giving <2.5% release after 4 h (Batista et al., 2021). In another study, tripeptides IPP and LKP loaded into CS nanoparticles showed 90 % release in simulated intestinal fluid (SIF) after 240 min and 75 % after 120 min in simulated gastric fluid (SGF) (Danish et al., 2017). Similarly, the tripeptide YKT loaded into CS nanoparticles showed release values of 26, 34, 43, and 97% after 8, 24, 48, and 264 h incubation in PBS buffer (pH 7.4) at 37 °C. The release kinetics were slower in CS + ALG nanoparticles; for example, the tripeptide KPV encapsulated into CS + ALG nanoparticles showed 25% at pH 6.2 after 30 min and increased to only 35% after 30 h (Laroui et al., 2010; Xiao et al., 2017). However, in none of these other studies do charge interactions of the peptides with the polymers themselves seem have been considered.

5. Conclusions

This study has shown the robust structural integrity of CS + ALG polymeric electrolyte complexes (PECs), particularly those formed at a molar charge ratio $(n^-/n^+) < 1$. Enhanced stability is observed in PECs with both excess CS and excess ALG in NaCl solution. The ionic

interaction between CS and ALG is more pronounced for higher Mw ALG molecules (21 kDa versus 8 kDa), resulting in more compact and stable PECs. The introduction of low Mw bioactive peptides (BAPs) into the CS + ALG PECs leads to a reduction in their hydrodynamic radius (R_h), with minimal impact on their ζ−potential and polydispersity, indicative of successful incorporation of the bioactives as well as their integration into and additional stabilization of the PEC structure. Encapsulation efficiency was high and release low in gastric and intestinal pH conditions, probably due to the stronger association between the oppositely charged BAP and ALG molecules. Thus, the simple one-step process of mixing CS, ALG and BAPs of appropriate charge represents a promising encapsulation technique for future industrial development, offering a sustainable approach for incorporating BAPs into gastrointestinal delivery vehicles.

CRediT authorship contribution statement

Yoni Atma: Writing – original draft, Visualization, Investigation, Funding acquisition, Formal analysis, Data curation. **Amin Sadegh-pour:** Writing – review & editing, Writing – original draft, Visualization, Validation, Supervision, Software, Methodology, Investigation, Formal analysis, Conceptualization. **Brent S. Murray:** Writing – review & editing, Writing – original draft, Visualization, Validation, Supervision, Project administration, Methodology, Formal analysis, Conceptualization. **Francisco M. Goycoolea:** Writing – review & editing, Writing – original draft, Visualization, Validation, Supervision, Project administration, Methodology, Formal analysis, Conceptualization.

Declaration of competing interest

The authors declare that they have no known competing financial interests or personal relationships that could have appeared to influence the work reported in this paper.

Acknowledgements

Appendix A. Supplementary data

Supplementary data to this article can be found online at https://doi.org/10.1016/j.foodhyd.2024.110789.

Data availability

Data will be made available on request.

References

Abdelhedi, O., Nasri, R., Mora, L., Toldrá, F., Nasri, M., & Jridi, M. (2017). Collagenous proteins from black-barred halfbeak skin as a source of gelatin and bioactive peptides. *Food Hydrocolloids, 70*, 123–133. https://doi.org/10.1016/j.foodhyd.2017.03.030

Aguilar-Toala, J. E., Quintanar-Guerrero, D., Liceaga, A. M., & Zambrano-Zaragoza, M. L. (2022). Encapsulation of bioactive peptides: A strategy to improve the stability, protect the nutraceutical bioactivity and support their food applications. *RSC Advances, 12*(11), 6449–6458. https://doi.org/10.1039/d1ra08590e

Alonso, M. J., & Goycoolea, F. M. (2008). Chitosan-polysaccharide blended nanoparticles for controlled drug delivery. In N. M. Neves, J. F. Mano, M. E. Gomes, A. P. Marques, & H. S. Azevedo (Eds.), *Natural-based polymers for biomedical applications* (pp. 644–679). Woadhead Publishing Ltd.

Anderson, W., Kozak, D., Coleman, V. A., Jamting, A. K., & Trau, M. (2013). A comparative study of submicron particle sizing platforms: Accuracy, precision and resolution analysis of polydisperse particle size distributions. *Journal of Colloid and Interface Science, 405*, 322–330. https://doi.org/10.1016/j.jcis.2013.02.030

Apostolidis, E., Stergiou, A., Kioupis, D., Sadeghpour, A., Paximada, P., Kakali, G., & Mandala, I. (2023). Production of nanoparticles from resistant starch via a simple three-step physical treatment. *Food Hydrocolloids, 137*. https://doi.org/10.1016/j.foodhyd.2022.108412

Atma, Y., Murray, B. S., Sadeghpour, A., & Goycoolea, F. M. (2024). Encapsulation of short-chain bioactive peptides (BAPs) for gastrointestinal delivery: A review. *Food & Function, 15*(8), 3959–3979. https://doi.org/10.1039/d3fo04195f

Basirico, L., Catalani, E., Morera, P., Cattaneo, S., Stuknyte, M., Bernabucci, U., De Noni, I., & Nardone, A. (2015). Release of angiotensin converting enzyme-inhibitor peptides during in vitro gastrointestinal digestion of Parmigiano Reggiano PDO cheese and their absorption through an in vitro model of intestinal epithelium. *Journal of Dairy Science, 98*(11), 7595–7601. https://doi.org/10.3168/jds.2015-9801

Batista, P., Castro, P. M., Madureira, A. R., Sarmento, B., & Pintado, M. (2021). Preparation, characterization and evaluation of guar films impregnated with relaxing peptide loaded into chitosan microparticles. *Applied Sciences, 11*(21). https://doi.org/10.3390/app11219849. Article 9849.

Becheran-Maron, L., Peniche, C., & Arguelles-Monal, W. (2004). Study of the interpolyelectrolyte reaction between chitosan and alginate: Influence of alginate composition and chitosan molecular weight. *International Journal of Biological Macromolecules, 34*(1–2), 127–133. https://doi.org/10.1016/j.ijbiomac.2004.03.010

Belitz, H. D., & Grosch, W. (1999). *Food chemistry* (2nd ed.). Springer-Verlag.

Bicak, B., Budama-Kilinc, Y., Kecel-Gunduz, S., Zorlud, T., & Akman, G. (2021). Peptide based nano-drug candidate for cancer treatment: Preparation, characterization, in vitro and in silico evaluation. *Journal of Molecular Structure, 1240*. https://doi.org/10.1016/j.molstruc.2021.130573

Cao, S., Wang, Y., Hao, Y., Zhang, W., & Zhou, G. (2020). Antihypertensive effects in vitro and in vivo of novel angiotensin-converting enzyme inhibitory peptides from bovine bone gelatin hydrolysate. *Journal of Agricultural and Food Chemistry, 68*(3), 759–768. https://doi.org/10.1021/acs.jafc.9b05618

Cazorla-Luna, R., Martin-Illana, A., Notario-Perez, F., Ruiz-Caro, R., & Veiga, M. D. (2021). Naturally occurring polyelectrolytes and their use for the development of complex-based mucoadhesive drug delivery systems: An overview. *Polymers, 13*(14). https://doi.org/10.3390/polym13142241

Cermeño, M., Kleekayai, T., Amigo-Benavent, M., Harnedy-Rothwell, P., & FitzGerald, R. J. (2020). Current knowledge on the extraction, purification, identification, and validation of bioactive peptides from seaweed. *Electrophoresis, 41* (20), 1694–1717. https://doi.org/10.1002/elps.202000153

Chen, S. X., Guo, F., Deng, T. T., Zhu, S. Q., Liu, W. Y., Zhong, H. J., Yu, H., Luo, R., & Deng, Z. Y. (2017). Eudragit S100-coated chitosan nanoparticles co-loading Tat for enhanced oral colon absorption of insulin. *AAPS PharmSciTech, 18*(4), 1277–1287. https://doi.org/10.1208/s12249-016-0594-z

Curtis, J. M., Dennis, D., Waddell, D. S., MacGillivray, T., & Ewart, H. S. (2002). Determination of angiotensin-converting enzyme inhibitory peptide Leu-Lys-Pro-Asn-Met (LKPNM) in bonito muscle hydrolysates by LC−MS/MS [Original Article]. *Journal of Agricultural and Food Chemistry, 50*, 3919–3925. https://doi.org/10.1021/jf011684c

Danish, M. K., Vozza, G., Byrne, H. J., Frias, J. M., & Ryan, S. M. (2017). Comparative study of the structural and physicochemical properties of two food derived antihypertensive tri-peptides, Isoleucine-Proline-Proline and Leucine-Lysine-Proline encapsulated into a chitosan based nanoparticle system. *Innov. Food Sci. Emerg., 44*, 139–148. https://doi.org/10.1016/j.ifset.2017.07.002

Doroszkowski, A. (1999). The physical chemistry of dispersion. In R. Lambourne, & T. A. Strivens (Eds.), *Paint and surface coatings: Theory and practice* (2nd ed. ed., pp. 198–242). Woodhead Publishing Limited.

Egger, L., Ménard, O., Delgado-Andrade, C., Alvito, P., Assunção, R., Balance, S., Barberá, R., Brodkorb, A., Cattenoz, T., Clemente, A., Comi, I., Dupont, D., Garcia-Llatas, G., Lagarda, M. J., Le Feunteun, S., JanssenDuijghuijsen, L., Karakaya, S., Lesmes, U., Mackie, A. R., … Portmann, R. (2016). The harmonized INFOGEST in vitro digestion method: From knowledge to action. *Food Research International, 88*, 217–225. https://doi.org/10.1016/j.foodres.2015.12.006

Estévez, N., Fuciños, P., Fuciños, C., Jauregi, P., Tovar, C. A., & Rúa, M. L. (2020). Hydrolysis of whey protein as a useful approach to obtain bioactive peptides and a β-Lg fraction with different biotechnological applications. *Food Hydrocolloids, 109*. https://doi.org/10.1016/j.foodhyd.2020.106095

Feng, K., Li, C., Wei, Y. S., Zong, M. H., Wu, H., & Han, S. Y. (2019). Development of a polysaccharide based multi-unit nanofiber mat for colon-targeted sustained release of salmon calcitonin. *Journal of Colloid and Interface Science, 552*, 186–195. https://doi.org/10.1016/j.jcis.2019.05.037

Fernández-Musoles, R., Salom, J. B., Castelló-Ruiz, M., Contreras, M.d. M., Recio, I., & Manzanares, P. (2013). Bioavailability of antihypertensive lactoferricin B-derived peptides: Transepithelial transport and resistance to intestinal and plasma peptidases. *International Dairy Journal, 32*(2), 169–174. https://doi.org/10.1016/j.idairyj.2013.05.009

Fuentea, B.d. l., Tornosa, A., Príncepa, A., Lorenzob, J. M., Pateirob, M., Berradaa, H., Barbaa, F. J., Ruiza, M.-J., & Martí-Quijal, F. J. (2020). Scaling-up processes: Patents and commercial applications. In J. M. Lorenzo, & F. J. Barba (Eds.), *Aquaculture and by-products: Challenges and opportunities in the use of alternative protein sources and bioactive compounds* (Vol. 92, pp. 187–223). Academic Press. https://doi.org/10.1016/bs.afnr.2019.12.003.

Fuenzalida, J. P., Nareddy, P. K., Moreno-Villoslada, I., Moerschbacher, B. M., Swamy, M. J., Pan, S., Ostermeier, M., & Goycoolea, F. M. (2016). On the role of

alginate structure in complexing with lysozyme and application for enzyme delivery. *Food Hydrocolloids, 53*, 239–248. https://doi.org/10.1016/j.foodhyd.2015.04.017

Fujita, H., Yokoyama, K., & Yoshikawa, M. (2000). Classification and antihypertensive activity of angiotensin I-converting enzyme inhibitory peptides derived from food proteins. *Journal of Food Science, 65*(4), 564–569. https://doi.org/10.1111/j.1365-2621.2000.tb16049.x

Fujita, H., & Yoshikawa, M. (1999). Lkpnm: A prodrug-type ACE-inhibitory peptide derived from fish protein. *Immunopharmacology, 44*, 123–127. https://doi.org/10.1016/s0162-3109(99)00118-6

Gao, R., Yu, Q., Shen, Y., Chu, Q., Chen, G., Fen, S., Yang, M., Yuan, L., McClements, D. J., & Sun, Q. (2021). Production, bioactive properties, and potential applications of fish protein hydrolysates: Developments and challenges. *Trends in Food Science & Technology, 110*, 687–699. https://doi.org/10.1016/j.tifs.2021.02.031

Gazzillo, D., Fantoni, R., & Giacometti, A. (2006). Phase behaviour of polydisperse sticky hard spheres: Analytical solutions and perturbation theory. *Molecular Physics, 104* (22–24), 3451–3459. https://doi.org/10.1080/00268970601050892

George, M., & Abraham, T. E. (2006). Polyionic hydrocolloids for the intestinal delivery of protein drugs: Alginate and chitosan–a review. *J Control Release, 114*(1), 1–14. https://doi.org/10.1016/j.jconrel.2006.04.017

Glantz, M., Hakansson, A., Lindmark Mansson, H., Paulsson, M., & Nilsson, L. (2010). Revealing the size, conformation, and shape of casein micelles and aggregates with asymmetrical flow field-flow fractionation and multiangle light scattering. *Langmuir, 26*(15), 12585–12591. https://doi.org/10.1021/la101892x

Gombotz, W. R., & Wee, S. F. (1998). Protein release from alginate matrices. *Advanced Drug Delivery Reviews, 31*, 267–285. https://doi.org/10.1016/S0169-409X(97)00124-5

Goycoolea, F. M., Lollo, G., Remunan-Lopez, C., Quaglia, F., & Alonso, M. J. (2009). Chitosan-alginate blended nanoparticles as carriers for the transmucosal delivery of macromolecules. *Biomacromolecules, 10*, 1736–1743. https://doi.org/10.1021/bm9001377

Goycoolea-Valencia, F. M., Morris, E. R., & Gidley, M. J. (1995). Screening for synergistic interactions in dilute polysaccharide solutions. *Carbohydrate Polymers, 28*(4), 351–358. https://doi.org/10.1016/0144-8617(95)00098-4

Guan, Z., Tjoeng, F. S., Li, W., Mandrell, K., Liu, M., & Chen, X. (2001). *Anti-hypertensive peptides (United States patent No. W. I. P. Organization).*

Guo, Q., Chen, P., & Chen, X. (2023). Bioactive peptides derived from fermented foods: Preparation and biological activities. *Journal of Functional Foods, 101*. https://doi.org/10.1016/j.jff.2023.105422

Hakansson, A., Ulmius, M., & Nilsson, L. (2012). Asymmetrical flow field-flow fractionation enables the characterization of molecular and supramolecular properties of cereal beta-glucan dispersions. *Carbohydrate Polymers, 87*(1), 518–523. https://doi.org/10.1016/j.carbpol.2011.08.014

Halim, N. R. A., Yusof, H. M., & Sarbon, N. M. (2016). Functional and bioactive properties of fish protein hydolysates and peptides: A comprehensive review. *Trends in Food Science & Technology, 51*, 24–33. https://doi.org/10.1016/j.tifs.2016.02.007

Han, R., Hernandez Alvarez, A. J., Maycock, J., Murray, B. S., & Boesch, C. (2021). Comparison of alcalase- and pepsin-treated oilseed protein hydrolysates - experimental validation of predicted antioxidant, antihypertensive and antidiabetic properties. *Current Research in Food Science, 4*, 141–149. https://doi.org/10.1016/j.crfs.2021.03.001

Han, R., Maycock, J., Murray, B. S., & Boesch, C. (2019). Identification of angiotensin converting enzyme and dipeptidyl peptidase-IV inhibitory peptides derived from oilseed proteins using two integrated bioinformatic approaches. *Food Research International, 115*, 283–291. https://doi.org/10.1016/j.foodres.2018.12.015

Harnedy, P. A., O'Keeffe, M. B., & FitzGerald, R. J. (2017). Fractionation and identification of antioxidant peptides from an enzymatically hydrolysed Palmaria palmata protein isolate. *Food Research International, 100*(Pt 1), 416–422. https://doi.org/10.1016/j.foodres.2017.07.037

Hayes, A., & Tiwari, B. K. (2015). Bioactive carbohydrates and peptides in foods: An overview of sources, downstream processing steps and associated bioactivities. *International Journal of Molecular Sciences, 16*, 22485–22508. https://doi.org/10.3390/ijms160922485

Hirai, A., Odani, H., & Nakajima, A. (1991). Determination of degree of deacetylation of chitosan by ^{1}H NMR spectroscopy. *Polymer Bulletin, (26)*, 87–94. https://doi.org/10.1007/BF00299352

Huang, G.-Q., Xiao, J.-X., Hao, L.-Q., & Yang, J. (2017). Microencapsulation of an angiotensin I-converting enzyme inhibitory peptide VLPVP by membrane emulsification. *Food Bioprocess Tech, 10*(11), 2005–2012. https://doi.org/10.1007/s11947-017-1953-9

Jiang, X. X., Pan, D. D., Tao, M. X., Zhang, T., Zeng, X. Q., Wu, Z., & Guo, Y. X. (2021). New nanocarrier system for liposomes coated with Lactobacillus acidophilus S-layer protein to improve Leu-Gln-Pro-Glu absorption through the intestinal epithelium. *J. Agr. Food Chem., 69*(27), 7593–7602. https://doi.org/10.1021/acs.jafc.1c01498

Jiang, B., Zhang, X., Yuan, Y., Qu, Y., & Feng, Z. (2017). Separation of antioxidant peptides from pepsin hydrolysate of whey protein isolate by ATPS of EOPO co-polymer (UCON)/phosphate. *Scientific Reports, 7*(1), Article 13320. https://doi.org/10.1038/s41598-017-13507-9

Kulkarni, A. D., Vanjari, Y. H., Sancheti, K. H., Patel, H. M., Belgamwar, V. S., Surana, S. J., & Pardeshi, C. V. (2016). Polyelectrolyte complexes: Mechanisms, critical experimental aspects, and applications. *Artificial Cells, Nanomedicine and Biotechnology, 44*(7), 1615–1625. https://doi.org/10.3109/21691401.2015.1129624

Kumar, P., Hajdu, C., Toth, A., & Horvath, D. (2021). Flow-driven surface instabilities of tubular chitosan hydrogel. *ChemPhysChem, 22*(5), 488–492. https://doi.org/10.1002/cphc.202000952

Kumar, M., Hasan, M., Choyal, P., Tomar, M., Gupta, O. P., Sasi, M., Changan, S., Lorenzo, J. M., Singh, S., Sampathrajan, V., Dhumal, S., Pandielvam, R., Satankar, V., Waghmare, R., Senapathy, M., Sayed, A. A. S., Radha, Dey, A., Amarowicz, R., & Kennedy, J. F. (2022). Cottonseed feedstock as a source of plant-based protein and bioactive peptides: Evidence based on biofunctionalities and industrial applications. *Food Hydrocolloids, 131*. https://doi.org/10.1016/j.foodhyd.2022.107776

Lacroix, I. M. E., Chen, X. M., Kitts, D. D., & Li-Chan, E. C. Y. (2017). Investigation into the bioavailability of milk protein-derived peptides with dipeptidyl-peptidase IV inhibition activity using Caco-2 cell monolayers. *Food Funct, 8*(2), 701–709. https://doi.org/10.1039/c6fo01411a

Laroui, H., Dalmasso, G., Nguyen, H. T., Yan, Y., Sitaraman, S. V., & Merlin, D. (2010). Drug-loaded nanoparticles targeted to the colon with polysaccharide hydrogel reduce colitis in a mouse model. *Gastroenterology, 138*(3), 843–853. https://doi.org/10.1053/j.gastro.2009.11.003. e841-842.

Le Gouic, A. V., Harnedy, P. A., & FitzGerald, R. J. (2019). Bioactive peptides from fish protein by-products. In *Bioactive molecules in food* (pp. 355–388). https://doi.org/10.1007/978-3-319-78030-6_29

Liu, Q., Yang, M., Zhao, B., & Yang, F. (2020). Isolation of antioxidant peptides from yak casein hydrolysate. *RSC Advances, 10*(34), 19844–19851. https://doi.org/10.1039/d0ra02644a

Lorenzo, J. M., Munekata, P. E. S., Gómez, B., Barba, F. J., Mora, L., Pérez-Santaescolástica, C., & Toldrá, F. (2018). Bioactive peptides as natural antioxidants in food products – a review. *Trends in Food Science & Technology, 79*, 136–147. https://doi.org/10.1016/j.tifs.2018.07.003

Luo, Y., & Wang, Q. (2014). Recent development of chitosan-based polyelectrolyte complexes with natural polysaccharides for drug delivery. *International Journal of Biological Macromolecules, 64*, 353–367. https://doi.org/10.1016/j.ijbiomac.2013.12.017

Ma, Z., Mondor, M., Goycoolea Valencia, F., & Hernandez-Alvarez, A. J. (2023). Current state of insect proteins: Extraction technologies, bioactive peptides and allergenicity of edible insect proteins. *Food Funct, 14*(18), 8129–8156. https://doi.org/10.1039/d3fo02865h

Marcet, I., Delgado, J., Diaz, N., Rendueles, M., & Diaz, M. (2022). Peptides recovery from egg yolk lipovitellins by ultrafiltration and their in silico bioactivity analysis. *Food Chemistry, 379*, Article 132145. https://doi.org/10.1016/j.foodchem.2022.132145

Menchicchi, B., Fuenzalida, J. P., Bobbili, K. B., Hensel, A., Swamy, M. J., & Goycoolea, F. M. (2014). Structure of chitosan determines its interactions with mucin. *Biomacromolecules, 15*(10), 3550–3558. https://doi.org/10.1021/bm5007954

Menchicchi, B., Fuenzalida, J. P., Hensel, A., Swamy, M. J., David, L., Rochas, C., & Goycoolea, F. M. (2015). Biophysical analysis of the molecular interactions between polysaccharides and mucin. *Biomacromolecules, 16*(3), 924–935. https://doi.org/10.1021/bm501832y

Milkova, V., & Goycoolea, F. M. (2020). Encapsulation of caffeine in polysaccharide oil-core nanocapsules. *Colloid and Polymer Science, 298*(8), 1035–1041. https://doi.org/10.1007/s00396-020-04653-0

Mohan, A., McClements, D. J., & Udenigwe, C. C. (2016). Encapsulation of bioactive whey peptides in soy lecithin-derived nanoliposomes: Influence of peptide molecular weight. *Food Chemistry, 213*, 143–148. https://doi.org/10.1016/j.foodchem.2016.06.075

Mohan, A., Rajendran, S. R. C. K., He, Q. S., Bazinet, L., & Udenigwe, C. C. (2015). Encapsulation of food protein hydrolysates and peptides: A review. *Rsc Advances, 5* (97), 79270–79278. https://doi.org/10.1039/c5ra13419f

Moreno-Fernández, J., Garcés-Rimón, M., & Miguel, M. (2020). Egg-derived peptides and hydrolysates: A new bioactive treasure for cardiometabolic diseases. *Trends in Food Science & Technology, 104*, 208–218. https://doi.org/10.1016/j.tifs.2020.08.002

Mudalige, T., Qu, H., Van Haute, D., Ansar, S. M., Paredes, A., & Ingle, T. (2019). Characterization of nanomaterials: Tools and challenges. In A. L. Rubio, M. m. R. Sanz, M. J. Fabra, & L. G. Gómez-Mascaraque (Eds.), *Nanomaterials for food applications* (pp. 313–353). Elsevier. https://doi.org/10.1016/b978-0-12-814130-4.00011-7.

Neves, A. C., Harnedy, P. A., O'Keeffe, M. B., & FitzGerald, R. J. (2017). Bioactive peptides from Atlantic salmon (Salmo salar) with angiotensin converting enzyme and dipeptidyl peptidase IV inhibitory, and antioxidant activities. *Food Chemistry, 218*, 396–405. https://doi.org/10.1016/j.foodchem.2016.09.053

Nilsson, L. (2013). Separation and characterization of food macromolecules using field-flow fractionation: A review. *Food Hydrocolloids, 30*(1), 1–11. https://doi.org/10.1016/j.foodhyd.2012.04.007

Nirmal, N. P., Santivarangkna, C., Rajput, M. S., Benjakul, S., & Maqsood, S. (2022). Valorization of fish byproducts: Sources to end-product applications of bioactive protein hydrolysate. *Comprehensive Reviews in Food Science and Food Safety, 21*(2), 1803–1842. https://doi.org/10.1111/1541-4337.12917

Nongonierma, A. B., Cadamuro, C., Le Gouic, A., Mudgil, P., Maqsood, S., & FitzGerald, R. J. (2019). Dipeptidyl peptidase IV (DPP-IV) inhibitory properties of a camel whey protein enriched hydrolysate preparation. *Food Chemistry, 279*, 70–79. https://doi.org/10.1016/j.foodchem.2018.11.142

Nongonierma, A. B., & FitzGerald, R. J. (2015). Bioactive properties of milk proteins in humans: A review. *Peptides, 73*, 20–34. https://doi.org/10.1016/j.peptides.2015.08.009

O'Connell, A., Gonzalez-Espinosa, Y., Goycoolea, F. M., Schuetz, P., & Mattsson, J. (2023). Characterisation of locust bean gum with asymmetric flow field-flow fractionation (AF4) and light scattering. *Carbohydrate Polymers, 322*, Article 121286. https://doi.org/10.1016/j.carbpol.2023.121286

O'Connell, A., Goycoolea, F. M., Gulotta, A., Holmqvist, P., Schuetz, P., & Mattsson, J. (2023). The structure and dynamics of locust bean gum in aqueous solution. *Food Hydrocolloid, 138*, Article 108446. https://doi.org/10.1016/j.foodhyd.2022.108446

O'Neill, G. J., Egan, T., Jacquier, J. C., O'Sullivan, M., & Dolores O'Riordan, E. (2015). Kinetics of immobilisation and release of tryptophan, riboflavin and peptides from whey protein microbeads. *Food Chemistry, 180*, 150–155. https://doi.org/10.1016/j.foodchem.2015.01.131

Patil, P. J., Usman, M., Zhang, C., Mehmood, A., Zhou, M., Teng, C., & Li, X. (2022). An updated review on food-derived bioactive peptides: Focus on the regulatory requirements, safety, and bioavailability. *Comprehensive Reviews in Food Science and Food Safety, 21*(2), 1732–1776. https://doi.org/10.1111/1541-4337.12911

Piovesana, S., Capriotti, A. L., Cavaliere, C., La Barbera, G., Montone, C. M., Zenezini Chiozzi, R., & Lagana, A. (2018). Recent trends and analytical challenges in plant bioactive peptide separation, identification and validation. *Analytical and Bioanalytical Chemistry, 410*(15), 3425–3444. https://doi.org/10.1007/s00216-018-0852-x

Potaś, J., Szymańska, E., & Winnicka, K. (2020). Challenges in developing of chitosan – based polyelectrolyte complexes as a platform for mucosal and skin drug delivery. *European Polymer Journal, 140*. https://doi.org/10.1016/j.eurpolymj.2020.110020

Pravinata, L., Akhtar, M., Bentley, P. J., Mahatnirunkul, T., & Murray, B. S. (2016). Preparation of alginate microgels in a simple one step process via the Leeds Jet Homogenizer. *Food Hydrocolloid, 61*, 77–84. https://doi.org/10.1016/j.foodhyd.2016.04.025

Raval, N., Maheshwari, R., Kalyane, D., Youngren-Ortiz, S. R., Chougule, M. B., & Tekade, R. K. (2019). Importance of physicochemical characterization of nanoparticles in pharmaceutical product development. In R. K. Tekade (Ed.), *Basic fundamentals of drug delivery* (pp. 369–400). Academic Press. https://doi.org/10.1016/b978-0-12-817909-3.00010-8.

Rinaudo, M., Milas, M., & Le Dung, P. (1993). Characterization of chitosan. Influence of ionic strength and degree of acetylation on chain expansion. *International Journal of Biological Macromolecules, 15*(5), 281–285. https://doi.org/10.1016/0141-8130(93)90027-J

Rinaudo, M., Pavlov, G., & Desbrières, J. (1999). Solubilization of chitosan in strong acid medium. *Int. J. Polym. Anal. Charac., 5*(3), 267–276. https://doi.org/10.1080/10236669908009742

Rinaudo, M., Pavlov, G., & Desbrières, J. (1999). Influence of acetic acid concentration on the solubilization of chitosan. *Polymer, 40*, 7029–7032.

Sæther, H. V., Holme, H. K., Maurstad, G., Smidsrød, O., & Stokke, B. T. (2008). Polyelectrolyte complex formation using alginate and chitosan. *Carbohydrate Polymers, 74*(4), 813–821. https://doi.org/10.1016/j.carbpol.2008.04.048

Schatz, C., Domard, A., Viton, C., Pichot, C., & Delair, T. (2004). Versatile and efficient formation of colloids of biopolymer-based polyelectrolyte complexes. *Biomacromolecules, 5*(5), 1882–1892. https://doi.org/10.1021/bm049786+

Schmidt, M., Nerger, D., & Burchard, W. (1979). Quasi-elastic light scattering from branched polymers: 1. Polyvinylacetate and polyvinylacetate—microgels prepared by emulsion polymerization. *Polymer, 20*(5), 582–588. https://doi.org/10.1016/0032-3861(79)90169-1

Sonaje, K., Chuang, E. Y., Lin, K. J., Yen, T. C., Su, F. Y., Tseng, M. T., & Sung, H. W. (2012). Opening of epithelial tight junctions and enhancement of paracellular permeation by chitosan: Microscopic, ultrastructural, and computed-tomographic observations. *Molecular Pharmaceutics, 9*(5), 1271–1279. https://doi.org/10.1021/mp200572t

Sousa, P., Borges, S., & Pintado, M. (2020). Enzymatic hydrolysis of insect Alphitobius diaperinus towards the development of bioactive peptide hydrolysates. *Food Funct, 11*(4), 3539–3548. https://doi.org/10.1039/d0fo00188k

Sreekumar, S., Wattjes, J., Niehues, A., Mengoni, T., Mendes, A. C., Morris, E. R., Goycoolea, F. M., & Moerschbacher, B. M. (2022). Biotechnologically produced chitosans with nonrandom acetylation patterns differ from conventional chitosans in properties and activities. *Nature Communications, 13*(1), 7125. https://doi.org/10.1038/s41467-022-34483-3

Stetefeld, J., McKenna, S. A., & Patel, T. R. (2016). Dynamic light scattering: A practical guide and applications in biomedical sciences. *Biophys Rev, 8*(4), 409–427. https://doi.org/10.1007/s12551-016-0218-6

Stewart, W. W., & Swaisgood, H. E. (1993). Characterization of calcium alginate pore diameter by size-exclusion chromatography using protein standards. *Enzyme and Microbial Technology, 15*(11), 922–927. https://doi.org/10.1016/0141-0229(93)90167-Z

Takeshita, S., Sadeghpour, A., Malfait, W. J., Konishi, A., Otake, K., & Yoda, S. (2019). Formation of nanofibrous structure in biopolymer aerogel during supercritical CO(2) processing: The case of chitosan aerogel. *Biomacromolecules, 20*(5), 2051–2057. https://doi.org/10.1021/acs.biomac.9b00246

Tanaka, H., Matsumura, M., & Veliky, I. A. (1984). Diffusion characteristics of substrates in Ca-alginate gel beads. *Biotechnology and Bioengineering, 26*(1), 53–58. https://doi.org/10.1002/bit.260260111

Trapani, A., Lopedota, A., Franco, M., Cioffi, N., Ieva, E., Garcia-Fuentes, M., & Alonso, M. J. (2010). A comparative study of chitosan and chitosan/cyclodextrin nanoparticles as potential carriers for the oral delivery of small peptides [Article]. *European Journal of Pharmaceutics and Biopharmaceutics, 75*(1), 26–32. https://doi.org/10.1016/j.ejpb.2010.01.010

Vold, I. M. N., Kristiansen, K. A., & Bjørn, E. C. (2006). A study of the chain stiffness and extension of alginates, in vitro epimerized alginates, and periodate-oxidized alginates using size-exclusion chromatography combined with light scattering and viscosity detectors. *Biomacromolecules, 7*(7), 2136–2146. https://doi.org/10.1021/bm060099n

Wattjes, J., Sreekumar, S., Richter, C., Cord-Landwehr, S., Singh, R., El Gueddari, N. E., & Moerschbacher, B. M. (2020). Patterns matter part 1: Chitosan polymers with non-random patterns of acetylation. *Reactive and Functional Polymers, 151*. https://doi.org/10.1016/j.reactfunctpolym.2020.104583

Xiao, B., Xu, Z., Viennois, E., Zhang, Y., Zhang, Z., Zhang, M., Han, M. K., Kang, Y., & Merlin, D. (2017). Orally targeted delivery of tripeptide KPV via hyaluronic acid-functionalized nanoparticles efficiently alleviates ulcerative colitis. *Molecular Therapy, 25*(7), 1628–1640. https://doi.org/10.1016/j.ymthe.2016.11.020

Xing, L., Liu, R., Cao, S., Zhang, W., & Guanghong, Z. (2019). Meat protein based bioactive peptides and their potential functional activity: A review. *International Journal of Food Science and Technology, 54*(6), 1956–1966. https://doi.org/10.1111/ijfs.14132

Yan, J., Zhao, J., Yang, R., & Zhao, W. (2019). Bioactive peptides with antidiabetic properties: A review. *Int. J. Food Sci. Tech., 54*(6), 1909–1919. https://doi.org/10.1111/ijfs.14090

Yilmaz, T., Maldonado, L., Turasan, H., & Kokini, J. (2019). Thermodynamic mechanism of particulation of sodium alginate and chitosan polyelectrolyte complexes as a function of charge ratio and order of addition. *Journal of Food Engineering, 254*, 42–50. https://doi.org/10.1016/j.jfoodeng.2019.03.002

Yokoyama, K., Chiba, H., & Yoshikawa, M. (1992). Peptide inhibitors for angiotensin I-converting enzyme from thermolysin digest of dried bonito. *Bioscience Biotechnology & Biochemistry, 56*(10), 1541–1545. https://doi.org/10.1271/bbb.56.1541

Yuan, H., Luo, Z., Ban, Z., Reiter, R. J., Ma, Q., Liang, Z., Yang, M., Li, X., & Li, L. (2022). Bioactive peptides of plant origin: Distribution, functionality, and evidence of benefits in food and health. *Food Funct, 13*(6), 3133–3158. https://doi.org/10.1039/d1fo04077d

Zamora-Sillero, J., Gharsallaoui, A., & Prentice, C. (2018). Peptides from fish by-product protein hydrolysates and its functional properties: An overview. *Marine Biotechnology, 20*(2), 118–130. https://doi.org/10.1007/s10126-018-9799-3

Zhang, S., Murray, B. S., Holmes, M., Ettelaie, R., & Sarkar, A. (2022). Gastrointestinal fate and fatty acid release of pickering emulsions stabilized by mixtures of plant protein microgels + cellulose particles: An in vitro static digestion study. *Food Biophysics, 18*(1), 120–132. https://doi.org/10.1007/s11483-022-09756-5

Zhang, S., Murray, B. S., Suriyachay, N., Holmes, M., Ettelaie, R., & Sarkar, A. (2021). Synergistic interactions of plant protein microgels and cellulose nanocrystals at the interface and their inhibition of the gastric digestion of pickering emulsions. *Langmuir, 37*(2), 827–840. https://doi.org/10.1021/acs.langmuir.0c03148

Zhang, Y. W., Tu, L. L., Tang, Z., Wang, Q., Zheng, G. L., & Yin, L. N. (2021). pH-sensitive chitosan-deoxycholic acid/alginate nanoparticles for oral insulin delivery. *Pharmaceutical Development and Technology, 26*(9), 943–952. https://doi.org/10.1080/10837450.2021.1966036

Zhou, J., Chen, M., Wu, S., Liao, X., Wang, J., Wu, Q., Zhuang, M., & Ding, Y. (2020). A review on mushroom-derived bioactive peptides: Preparation and biological activities. *Food Research International, 134*, Article 109230. https://doi.org/10.1016/j.foodres.2020.109230